JCTC Journal of Chemical Theory and Computation

Multiconfigurational Second-Order Perturbation Theory Restricted Active Space (RASPT2) Method for Electronic Excited States: A Benchmark Study

Vicenta Sauri,[†] Luis Serrano-Andrés,[†,⊥] Abdul Rehaman Moughal Shahi,[‡] Laura Gagliardi,*[,§] Steven Vancoillie,[||] and Kristine Pierloot*[,||]

Instituto de Ciencia Molecular, Universitat de València, P.O. Box 22085, ES-46071 Valencia, Spain, Department of Physical Chemistry, University of Geneva, 30, q. E. Ansermet, 1211 Genève, Switzerland, Department of Chemistry and Supercomputing Institute, University of Minnesota, 207 Pleasant St. SE, Minneapolis, Minnesota 55455-0431, United States, and Department of Chemistry, Katholieke Universiteit Leuven, Belgium

Received August 24, 2010

Abstract: The recently developed second-order perturbation theory restricted active space (RASPT2) method has been benchmarked versus the well-established complete active space (CASPT2) approach. Vertical excitation energies for valence and Rydberg excited states of different groups of organic (polyenes, acenes, heterocycles, azabenzenes, nucleobases, and free base porphin) and inorganic (nickel atom and copper tetrachloride dianion) molecules have been computed at the RASPT2 and multistate (MS) RASPT2 levels using different reference spaces and compared with CASPT2, CCSD, and experimental data in order to set the accuracy of the approach, which extends the applicability of multiconfigurational perturbation theory to much larger and complex systems than previously. Relevant aspects in multiconfigurational excited state quantum chemistry such as the valence−Rydberg mixing problem in organic molecules or the double d-shell effect for first-row transition metals have also been addressed.

Introduction

The development and efficient implementation of the multiconfigurational second-order perturbation theory approach (CASPT2) in the beginning of the 1990s by Roos and coworkers[1] represented a breakthrough for quantum chemistry in general, but more specifically for the study of those electronic structure cases which required a multiconfigurational description of the reference wave function. Those problems were then first solved quantitatively or accurately in many polyatomic systems, such as a number of bond breakings and dissociations,[2] potential energy hypersurface (PEH) degeneracies (conical intersections),[3] symmetry breaking problems (Cope rearrangement),[4] biradical situations,[5,6] organic molecules photophysics,[7−10] transition metal (TM) bonding[11−16] and spectroscopy,[17−22] and actinide chemistry.[23−26]

In particular, this method showed to be best suited to deal with the quantum chemistry of the excited state.[27] For the first time, the overall level of accuracy in the determination of electronic excitation energies in small- to medium-sized molecules reached 0.1−0.3 eV for systems up to 30 atoms, like free base porphin.[28] The ability of a multiconfigurational approach that extensively includes correlation effects like the CASPT2 method opened the door for studying spectroscopic and photochemical phenomena in systems in which computationally more costly approaches such as multireference configuration interaction (MRCI) could not be applied. In a recent benchmark study of excitation energies in organic molecules,[29] the current version of the CASPT2 method—in which the IPEA zeroth-order Hamiltonian[30] was used—was

* Corresponding authors. E-mail: gagliard@umn.edu (L.G.); Kristin.Pierloot@chem.kuleuven.be (K.P.).
[†] Universitat de València.
[‡] University of Geneva.
[§] University of Minnesota.
[||] Katholieke Universiteit Leuven.
[⊥] Deceased, September 2010.

10.1021/ct100478d
Published on Web 12/08/2010

shown to be superior to the CCSD and CC2 approaches and equally as accurate as the linear response coupled-cluster CC3 procedure for closed-shell ground-state systems. CASPT2 has also proven to be much better than any other method in medium-sized molecules for excited states in cases where the ground state is poorly defined by a closed-shell configuration (biradicals, conical intersections, dissociation paths) or the excited state has a strong multiconfigurational or diexcited character.[29,31]

The CASPT2 method is, however, not free of drawbacks, all of them actually related with the limitation in the size of the complete active space (CAS) due to the difficulties in handling large high-order density matrices. Some of the weaknesses of the CASPT2 method which were partially solved were (i) the intruder state problem perturbing the first-order interacting reference space—which required the introduction of a level-shift correction (LS-CASPT2);[32,33] (ii) the overestimation of high-multiplicity states—solved by the IPEA zeroth-order Hamiltonian;[30] (iii) the lack of orthogonality of the individual single-state CASPT2 solutions, causing improper mixing of valence and Rydberg wave functions[7] or unphysical state crossings[34]—which was solved by developing the multistate (MS) CASPT2 approach.[35] These weaknesses generally affected the size and accuracy of the problems under study because the maximum active space size of 13−15 molecular orbitals (MOs) was rapidly reached, especially if a large number of Rydberg orbitals has to be considered. Specific problems like, for instance, the need to include in the CAS a second d-shell (4d) for first-row transition metal atoms were also soon recognized.[36]

As mentioned, all of these problems have one straightforward solution: increasing the active space size. Recent methodological developments in *ab initio* quantum chemistry like the Cholesky decomposition (CD) approach, also implemented for the CASPT2 method,[37,38] have reduced the effort involved in handling two-electron integrals and have extended the applicability of *ab initio* methods to much larger molecular systems. For instance, a 1000 basis set CD-CASPT2 calculation is easily affordable nowadays within the MOLCAS package.[38−41] Truncation of the virtual space in CD-CASPT2 calculations is also possible.[42] This method is based on a modified version of the frozen natural orbital (FNO) approach used in coupled cluster theory. However, increasing the molecular size or truncating the virtual space are not always sufficient techniques. There are many quantum-chemical problems whose accurate solution is out of reach for CASPT2 because the adequate number of MOs cannot be included in the active space, like organometallic systems with more than one transition metal atom, extended π-space molecules with more than 14 π MOs, problems in which the inclusion of additional σ MOs is needed, or chemical reactions in which the requirements for a balanced space exceeds the capability of the CAS approach.

The recent implementation of the second-order perturbation theory restricted active space (RASPT2) method leads the field in the proper direction.[43] In the CAS framework,[44] the MO space is divided into three subspaces with a varying number of electrons: inactive (always doubly occupied), active (with varying occupation from zero to two), and secondary (always empty). All possible excitation levels compatible with spatial and spin symmetry involving the electrons in the active space form the multiconfigurational CAS-CI space used as a reference for a further perturbative CASPT2 treatment.[1,2] The configurational space rapidly grows to many millions of determinants with the size of the active space, making the treatment unaffordable. The RAS method[45,46] further divides the active space into three subspaces: RAS1, RAS2, and RAS3. The final multireference space is built by allowing in RAS2 the same type of full-CI expansion as previously in CAS, but restricting in RAS1 and RAS3 the excitation level to a predefined range: up to single (S), double (SD), triple (SDT), quadruple (SDTQ), etc., by limiting the number of allowed holes (RAS1) and particles (RAS3). Avoiding high excitation levels in RAS1 and RAS3 leads to less extended multiconfigurational spaces, therefore allowing a much larger number of active orbitals as compared with the CAS expansions. However, the number of possible divisions of the active space combined with the different allowed levels of excitation increases the choices of configurational expansions and the number of solutions, thus making the RASSCF/RASPT2 method less systematic than the CASSCF/CASPT2 method.

The selection of RAS spaces requires very careful calibration. Finding reliable strategies for general purpose calculations is highly required. Up to now, the RASPT2 method has been tested in the determination of the singlet−triplet state energy splitting of three copper−dioxygen and two copper−oxo complexes[43,47] and one-electron ionization potential and optical band gaps of ethylene, acetylene, and phenylene oligomers.[48] It has been shown how RASPT2 offers a similar accuracy when compared to CASPT2 at significantly reduced computational expense, whereas more demanding calculations out of reach for CASPT2 can be performed with the new formulation.

In the present contribution, we focus on electronic excitation energies, a field in which RASPT2 probably will play a major role in the coming years. We have selected different sets of molecules in order to check the accuracy of the method and the computational strategies in systems and problems of various classes, including valence and Rydberg, singlet and triplet, and ligand-field and charge-transfer excited states in different organic and inorganic systems. Figure 1 compiles the benchmark set of molecules considered in the present study.

The paper is divided into four sections, each of which focuses on one aspect of the calibration. Initially, free base porphin will be used as an example of the use of RASPT2 in a system with an extended π system whose inclusion in the active space is out of reach for CASPT2. Then, excitation energies of singlet and triplet valence and Rydberg states of ethene and benzene will be computed in order to test the accuracy and ability of RASPT2 to deal with the simultaneous calculation of valence and Rydberg states, and how it takes care of the valence−Rydberg problem. Next, the valence states of naphthalene and a set of organic five- and six-membered heterocyclic molecules and DNA/RNA nucleobases will be computed with RASPT2 to determine the accuracy of the results with different partitions of the RAS

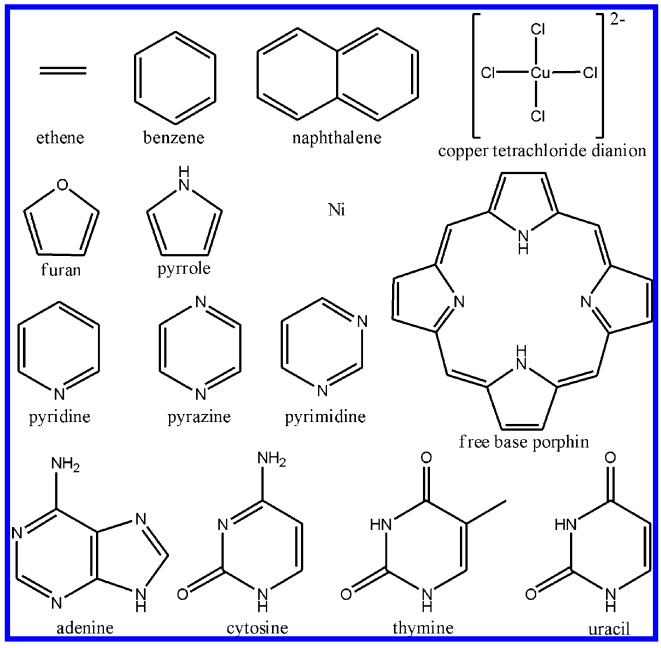

Figure 1. Benchmark set of molecules considered in this study.

space. Finally, the nickel atom and the copper tetrachloride dianion will be computed in order to establish the accuracy and proper strategies required in RASPT2 to handle the required inclusion of a second correlating d shell for first-row transition metal compounds, and how the new method simplifies the calculations and extends their possibilities.

2. Computational Details

All CASSCF/CASPT2 and RASSCF/RASPT2 calculations were performed with the MOLCAS-7 program.[39] All-electron, one-electron basis sets were used throughout. For ethene and benzene (and except when indicated), the calculations were performed with an ANO-L basis set[49] contracted to [4s3p1d] for carbon and [2s1p] for hydrogen atoms. In addition, 1s-type, 1p-type, and 1d-type contracted functions, with diffuse coefficients described elsewhere,[35] were added to this basis set and placed in the center of the molecule to describe Rydberg orbitals. For free base porphin, an ANO-S C,N[3s2p1d]/H[2s] basis set was used. For all other organic systems, a triple-ζ valence polarized basis (TZVP) set was employed.[50] Cholesky decomposition of the two-electron integrals was accomplished with a threshold of 10^{-5} au.[51] Reduced-scaling evaluation of the Fock exchange matrices in the CASSCF and RASSCF calculations was accomplished by means of the Local-K screening approach[52] employing localized Cholesky orbitals.[53] For the calculations on transition metal systems, ANO-RCC basis sets[54] were used, contracted to [7s6p4d3f2g] for nickel, [7s6p4d3f2g1h] for copper, and [5s4p2d1f] for chlorine atoms. Scalar relativistic effects were included using a Douglas−Kroll−Hess Hamiltonian.[55,56] In ethene and benzene, except when mentioned, the ground state geometries were taken from gas-phase experimental determinations, as described in the Supporting Information (SI). $CuCl_4^{2-}$ is square-planar (D_{4h}), and the Cu−Cl distance, 2.291 Å, was taken from our previous study.[57] The other systems were optimized with density functional theory (DFT) and the B3LYP functional[58] using the Turbomole 5.10 package and employing the triple-ζ valence polarized basis sets available in Turbomole.[59] At the optimized geometries, subsequent single point MS-CASSCF/CASPT2 and MS-RASSCF/RASPT2 calculations were performed using the mentioned basis sets. When high symmetry is required, for instance, D_{6h} in benzene, D_{4h} for $CuCl_4^{2-}$, or spherical symmetry in the nickel atom, the calculations were performed in a lower-symmetry point group, and MOLCAS tools were used to obtain the proper orbital symmetry. An imaginary level shift[32] of 0.1 au was used to prevent weakly coupling intruder states' interference, and the default shift for the IPEA zeroth-order Hamiltonian[30] (0.25 au) was employed. The value of 0.25 au is now the default in CASPT2, and we have used it in all cases, except for the free base porphin calculations where we have set the shift equal to zero. The reason for this different choice is that we wanted to compare the present results to those obtained prior to the introduction of the IPEA shift in 2004.[28,60] However this study does not focus on IPEA shift effects, and we do not compare results with different IPEA shifts for each system because this deviates from the purpose of the present study. In all calculations, the core electrons are kept frozen in the perturbative calculations, except for the nickel atom where the 3s and 3p electrons are included.

It is important to describe the notation employed to label CAS and RAS calculations. In the first case, the traditional label is used, that is, CAS(n,i), where n is the number of electrons included in the active space and i is the number of active orbitals. For RAS calculations, a longer notation is used, RAS(n,l,m;i,j,k), where n is the number of active electrons, l the maximum number of holes allowed in RAS1, and m the maximum number of electrons to enter in RAS3. Active orbitals are labeled by i,j,k and refer to those placed in RAS1, RAS2, and RAS3, respectively. Sometimes, we will also use S, SD, SDT, or SDTQ to emphasize the maximum RAS1→RAS3 excitation level. The RAS2 subspace has the same meaning in RASSCF as the CAS active space in a CASSCF calculation; i.e., all possible spin- and spatial symmetry-adapted configuration state functions (CSFs) that can be constructed from the orbitals in RAS2 are included in the multiconfigurational wave function. The RAS1 and RAS3 subspaces, on the other hand, permit the generation of additional CSFs subject to the restriction that a limited number of excitations may occur from RAS1, which otherwise contains only doubly occupied orbitals, and a limited number of excitations may occur in RAS3, which otherwise contains only empty orbitals. The active space employed for the various systems will be described in each section. Further details are reported in the SI .

3. Results and discussion

3.A. Free Base Porphin. Free base porphin (FBP) is an example of an extended π-conjugated system having 26 valence $\pi\pi^*$ electrons and 24 $\pi\pi^*$ MOs (26/24). Including a full $\pi\pi^*$ active space is out of reach for a conventional CASPT2 calculation. Previous studies were performed at the CASPT2(4/4) and CASPT2(16/14) levels.[28,60] In the former

Table 1. Excitation Energies (eV) of the Singlet and Triplet Valence $\pi\pi^*$ States of Free Base Porphin (D_{2h})

state	CASPT2 (4/4)[a]	CASPT2 (16/14)[b]	RASPT2 (26,2,2;11,4,9) (SD)[c]	RASPT2 (26,3,3;11,4,9) (SDT)[c]	RASPT2 (26,2,2;i,j,k) (SD)[d]	STEOM-CCSD[e]	exptl[f]
1^1B_{3u}	1.70	1.63	2.18	1.91	2.18	1.75	1.98 − 2.02 (Q_x)
1^1B_{2u}	2.26	2.11	2.38	2.16	2.38	2.40	2.33 − 2.42 (Q_y)
2^1B_{2u}	2.91	3.08	3.23	2.86	3.23	3.62	3.13 − 3.33 (B)
2^1B_{3u}	3.04	3.12	3.21	3.16	3.21	3.47	3.13 − 3.33 (B)
3^1B_{2u}		3.42	5.22 (3.30)[g]	3.37	3.80	4.35	3.65 (N)
3^1B_{3u}		3.53	5.38 (3.21)[g]	3.28	3.48	4.06	3.65 (N)
4^1B_{2u}		3.96	5.95 (4.02)[g]	4.10	4.20	5.00	4.25 (L)
4^1B_{3u}		4.04	6.04 (4.14)[g]	4.22	4.23	5.17	4.25 (L)
1^3B_{2u}		1.52	1.83	1.70	1.83	1.26	1.58
1^3B_{3u}		1.85	1.99	1.77	1.99	1.80	
2^3B_{3u}		1.88	1.98	1.88	1.98	1.98	
2^3B_{2u}		1.98	1.98	1.90	1.98	1.85	
CSF[h]	8	537705	63258 (1877432)[g]	1877565	279974/676297		

[a] CASPT2(4,4)/ANO-L 3s2p/2s, ref 60. Gouterman's four-electron/four-MO CAS space. [b] CASPT2(16,14)/ANO-S 3s2p1d/2s, ref 28. [c] Present RASPT2 results. Full $\pi\pi^*$ 26-electron/24-MO RAS employed. Gouterman's 4/4 space placed in RAS2. SD or SDT for all states except when indicated. The poor results for the highest singlet states explained in the text. [d] Different RAS spaces partition following the occupation number criterion of Table 2. See text. [e] STEOM-CCSD/SVZP results from ref 61. [f] See data in ref 28. [g] Present RASPT2 results. Full $\pi\pi^*$ 26-electron/24 MO-RAS employed. Gouterman's 4/4 space placed in RAS2. Within parentheses are results using SD for the ground 1^1A_g state and SDT for the excited state and CSFs for the excited-state $^1B_{2u}$ SDT calculations. [h] Number of configuration state functions (CSF) for the ^1A_g symmetry. In the sixth column are CSFs for active spaces (26,2,2;8,6,9)(SD)/(26,2,2;6,8,9)(SD) as examples.

Table 2. Natural Occupation Numbers of the Most Relevant Molecular Orbitals of the Low-Lying $\pi\pi^*$ States of Free Base Porphin (D_{2h})[a]

state	$3b_{1u}$	$4b_{1u}$	$2b_{2g}$	$3b_{2g}$	$3b_{3g}$	$5b_{1u}$[b]	$2a_u$[b]	$4b_{2g}$[b]	$4b_{3g}$[b]	$3a_u$	RAS2[c] $b_{1u}b_{2\ g}b_{3\ g}a_u/e^-$
1^1A_g	1.9692	1.9596	1.9714	1.9561	1.9581	1.8539	1.8631	0.1481	0.1595	0.0543	
1^1B_{3u}	1.9699	1.9606	1.9349	1.9715	1.9646	1.4726	1.4449	0.5448	0.5664	0.0739	1111/4
1^1B_{2u}	1.9696	1.9622	1.9702	1.9601	1.9625	1.5462	1.3962	0.6117	0.4803	0.0626	1111/4
2^1B_{2u}	1.9609	1.9684	1.9662	1.9582	1.9638	1.3169	1.4744	0.5389	0.6988	0.0615	1111/4
2^1B_{3u}	1.9713	1.9527	1.9526	1.9722	1.9451	1.3941	1.4197	0.6275	0.6037	0.0602	1111/4
3^1B_{2u}	1.9906	1.2519	1.9907	1.9637	1.7919	1.7860	1.7749	0.2467	1.0048	0.0992	2121/8
3^1B_{3u}	1.9922	1.3057	1.9617	1.9923	1.7339	1.8496	1.6622	1.1639	0.1479	0.0773	2121/8
4^1B_{2u}	1.2515	1.9914	1.7929	1.9747	1.9898	1.8367	1.7494	0.1429	1.0928	0.0765	3311/10
4^1B_{3u}	1.3231	1.9910	1.9694	1.7753	1.9894	1.8312	1.6278	0.9479	0.2936	0.1310	3312/10

[a] RASSCF(26,2,2;11,4,9)(SD) level of calculation. [b] Orbitals of the 4/4 Gouterman's space. [c] Orbitals and electrons within RAS2 selected from the occupation numbers (<1.9 and >0.1).

case, only four singlet states were computed, whereas eight singlet and eight triplet states were obtained at the latter level of theory. An overall agreement of 0.2−0.3 eV with respect to experimental values was obtained for all eight singlet states belonging to the porphin Q, B, N, and L bands, although in all these cases, CASPT2 yields too low values. FBP will be employed as a typical example of how to properly select the RAS active spaces and establish a RAS1/RAS3 excitation level yielding balanced and accurate excitation energies.

Table 1 displays a comparison between our new RASPT2 calculations and the previous CASPT2 calculations. The former includes all $\pi\pi^*$ valence electrons and MOs (26/24) in the RAS active space. As in many other organic molecules, the two highest-lying occupied MOs (HOMO and HOMO−1) and the two lowest-lying MOs (LUMO and LUMO+1) are the four most relevant MOs to describe the four lowest-lying states of the molecule.[27] This active space (named Gouterman's space in FBP) was previously used for CASPT2 calculations and showed to be necessary to describe the nature of such states. Indeed, CASPT2(4/4) calculations (see Table 1) provided reasonably accurate values for the mentioned states, as well as CASPT2(16/14), including Gouterman's MOs plus other additional orbitals which allowed calculation of higher roots.

How should we find out how to partition the RAS spaces in order to include FBP full $\pi\pi^*$ space and obtain accurate results? Not all partitions are equally adequate, and especially the choice of RAS2 has to be made carefully. Table 2 summarizes the natural orbital occupation numbers for a number of relevant MOs obtained in a RASSCF(26,2,2;11,4,9)(SD) calculation. This level of theory, including the four Gouterman's MOs in RAS2, the remaining $\pi\pi^*$ occupied and unoccupied MOs in RAS1 and RAS3, respectively, and up to double excitations (SD) for the latter spaces, is not intended to get accurate results for all nine computed states but just to guide us in designing the RAS partition. For each excited state, we have selected (see last column in Table 2) the most relevant MOs, namely, those in which the occupation number is below 1.9 or above 0.1. Obviously such a number may vary at the different RASSCF levels, but just slightly. It is shown, for instance, that for the four lowest-lying states just the four Gouterman's MOs fulfill such requirements, as expected, whereas two more occupied MOs are required for the 3^1B_{2u} and 3^1B_{3u} states and two and three more for the 4^1B_{2u} and 4^1B_{3u} states, respectively.

Why is this analysis so important? In order to have a balanced and accurate energy difference between states, the MOs strongly differing in occupation number for such states must be placed in RAS2 simultaneously. That is, to get

balanced RASPT2 excitation energies from the ground to the 1^1B_{2u}, 2^1B_{2u}, 1^1B_{3u}, and 2^1B_{3u} excited states, at least the four Gouterman's MOs ($b_{1u}b_{2g}b_{3g}a_u/n_e$;1111/4) must be placed in RAS2. Otherwise the description of the various states will be strongly unbalanced at the initial RASSCF level, and RASPT2 may not be able to recover the desired accuracy. This is better seen in the case of the higher-lying states. In Table 1, we report excitation energies at the RASPT2(26,2,2;11,4,9)(SD) level of calculation. Only the four Gouterman's MOs are included in RAS2, and single and double excitations (SD) are allowed from RAS1 to RAS3 to obtain the RAS-CI expansion. This level is clearly adequate for describing the four lowest-lying states, largely reducing the computational cost with respect to CASPT2(16/14) (only 10% of CSFs required for the RAS calculations). The case is quite different for the four next states, which require additional MOs to be properly described (see Table 2).

The RASPT2 excitation energies deviate toward high values by more than 1.5 eV, showing the underestimation of the correlation energy for the excited states as compared with the ground state. In parentheses, we included the results of increasing the CI excitation level only for the excited states to SDT, while keeping SD for the ground state, a strategy that partially restores the lost balance, giving excitation energies within 0.2−0.3 eV from the experimental values. Similar results are obtained if we increase the level of excitation in RAS1/RAS3 to triple excitations for all states with the RASPT2 (26,3,3;11,4,9)(SDT) calculations, proving that the ground state treatment does not improve with respect to the SD level. In any case, the computational cost increases enormously by including the triple excitations (30 times more CSFs are required).

We also performed more elaborate calculations in which each pair of states (here, the ground and each excited state) has been computed using the specific active space suggested by the occupation numbers in Table 2. In this procedure, both the ground and excited states have in RAS2 those MOs largely changing their occupation number in the excitation process. These calculations (which are equivalent to the RASPT2(26,2,2;11,4,9)(SD) results for the four lowest-lying states) provide the most accurate set of results for the different states at an intermediate computational cost.

The main conclusion obtained from these sets of calculations on FPB is that RASPT2 can provide accurate results for excited states only if the design of the RAS partition, and particularly the composition of the RAS2 space, is carefully controlled. RAS2 must contain those MOs that largely change their occupation number in the states under comparison. Otherwise, the corresponding states will have an unbalanced CI description, and perturbation theory might be unable to provide accurate excitation energies. Any initial RASSCF SD calculation on the requested states including a large enough active space will be sufficient to identify the MOs that should be placed in RAS2, and the occupation number criterion (<1.9 and >0.1) can be used for guidance. If the RAS2 partition is correct, the singles and doubles (SD) level of CI excitation required in RAS1 and RAS3 is sufficient to provide accurate excitation energies at a reasonable computational cost. Increasing the excitation level (triple or quadruple CIs) may partially compensate for the lack of balance, but it typically gives large CI expansions that may become very expensive. The use of the full $\pi\pi^*$ 26/24 active space increases the accuracy compared to more limited active spaces. Furthermore, RASPT2 compares well with experimental results, unlike CCSD, especially for the higher states, which deviate from experimental results by almost 0.8 eV at the CCSD level of calculation. RASSCF/RASPT2 can therefore be considered a very convenient tool for studying the spectrum of this type of π-extended system. This is even more important when carrying out geometry optimizations. Occasionally, the selective partition of a large π space like that of porphin leads to localized solutions at the CASSCF level, which can be avoided at the RASSCF level, as shown recently in psoralen.[62]

3.B. Ethene and the Valence−Rydberg Mixing Problem. Ethene is usually described by two $\pi\pi^*$ valence orbitals—the HOMO (highest occupied molecular orbital) and LUMO (lowest unoccupied molecular orbital)—that form the basis for the low-lying valence singlet and triplet $\pi\pi^*$ states. Additionally, series of diffuse states of increasing energies converging to the ionization potentials (IPs) of the molecule, named the Rydberg states, will also appear at low energies in the gas-phase absorption spectrum. To represent such states, we have employed, as previously done,[35,63] a specific atomic-type one-electron basis set of diffuse character placed on the molecular centroid. The lowest Rydberg series will be represented by excitations (basically single excitations) from the HOMO orbital to each of the orbitals of the $n = 3$ series, 3s3p3d, where n has a value one unit more than the valence main quantum number. As the required valence $\pi\pi^*$ active space is small, previous studies at the CASPT2 level[35,63] employed an active space of two electrons in 11 orbitals, including the two valence $\pi\pi^*$ plus the nine 3s3p3d Rydberg orbitals. As was soon detected in polyenes,[63] the CASSCF procedure is unable to deal properly with the simultaneous calculation of valence and Rydberg states. The lack of correlation leads to wave functions in which the MOs are strongly mixed—the so-called valence-Rydberg mixing—yielding too diffuse valence states and too compact Rydberg orbitals that only the multistate CASPT2 is able to correct. Compared with these previous calculations, the RASPT2 results in Table 3 can help us to answer several questions. First, is there any simple partition of the active space that avoids the costly inclusion of the Rydberg orbitals within the CAS space? Second, what is the origin of the valence−Rydberg mixing, and how does RASPT2 handle this problem? Finally, is the multistate treatment still needed, and is there any affordable additional solution?

As observed in Table 3, and in previous studies,[63] for the lowest-energy $^1B_{1u}$ states, the perturbative CASPT2(2,11) correction produces values off by almost 0.5 eV compared to experimental results. The analysis of the orbital extension $\langle r^2 \rangle$ (see that elsewhere)[35] indicates that even when for the lowest-energy state it should reflect its valence and compact character, yielding a similar value to that for the ground state (1^1A_g), the magnitude for the orbital extension is almost 4 times larger for both excited states, an illustration of the

Table 3. Excitation Energies (eV) of Selected States of Ethene (D_{2h})[a]

			S		SDT		
state	CASPT2 (2,11)[b]	MS-CASPT2 (2,11)[b]	RASPT2[c] (2,0,1;0,2,9)	MS-RASPT2[c] (2,0,1;0,2,9)	RASPT2[d] (12,3,3;5,2,16)	MS-RASPT2[d] (12,3,3;5,2,16)	exptl[e]
$1^1B_{1u}(\pi\pi^*)$	8.43	8.04	8.44	8.13	8.06	8.00	8.0[f]
$2^1B_{1u}(3d\pi)$	8.98	9.38	9.03	9.35	9.35	9.41	9.33

[a] Comparison of CASPT2, MS-CASPT2, RASPT2, and MS-RASPT2 results with $\pi\pi^*$ plus Rydberg and $\pi\pi^*$ and $\sigma\sigma^*$ plus Rydberg active spaces. [b] CASPT2 and MS-CASPT2, from a state average of two $^1B_{1u}$ roots and a two-electron−11-orbital including the two $\pi\pi^*$ MOs and nine ($n = 3$) Rydberg MOs. [c] RASPT2 and MS-RASPT2, from a state average of two $^1B_{1u}$ roots and a two-electron−11-orbital including the two $\pi\pi^*$ MOs (in RAS2) and nine ($n = 3$) Rydberg MOs (in RAS3). Only one particle is allowed (S excitations) in RAS3. [d] RASPT2 and MS-RASPT2, from a state average of three $^1B_{1u}$ roots and a 12-electron−16-orbital including the two $\pi\pi^*$ (in RAS2) MOs, five $\sigma\sigma^*$ MOs (RAS1 and RAS3), and nine ($n = 3$) Rydberg MOs (in RAS3). [e] Experimental data. See ref 7. [f] Estimated vertical excitation energy from earlier theoretical work. See therein, ref 63.

mixed character of the obtained wave function. It was already proven[35] that the use of the MS-CASPT2 level of calculation is required to get a correct result for the interacting $^1B_{1u}$ states and solve the so-called valence−Rydberg mixing problem. After the orthogonalization produced by the MS treatment, the valence and Rydberg states are clearly separated, and the corresponding orbital extension—computed by using the perturbatively-modified CAS-CI (PMCAS-CI) wave function obtained from the MS method—decreases close to the ground state value for the valence 1^1B_{1u} state, whereas it largely increases for the Rydberg 2^1B_{1u} states.

In the RASPT2 calculations, we have followed two types of computational strategies. First, we have placed the nine Rydberg MOs into the RAS3 active space, leaving the RAS1 space empty and the two $\pi\pi^*$ valence MOs and electrons in RAS2. We have allowed only combined single excitations toward RAS3, since the Rydberg states are typically well described just by single one-electron promotions, as previously suggested.[64] The active space employed can be labeled as RASPT2(2,0,1;0,2,9)(S), including two active electrons and 11 MOs. Table 3 shows that at such a level of calculation, that is, by moving the Rydberg MOs to RAS3, there is no loss of accuracy compared to CASPT2(2,11)/MS-CASPT2(2,11). In this small system, the computational effort is only marginally decreased, but the gain will be much more important in larger molecules. Furthermore, two more advantages can be highlighted: additional valence MOs can eventually be added to RAS2 if required for larger systems, and a single partition of the active space is made available, simplifying considerably the calculations. On the other hand, the behavior of CASPT2(2,11) and RASPT2(2,0,1;0,2,9)(S) with respect to the valence−Rydberg mixing problem is basically the same, as could be expected by the fact that the same types of correlation effects ($\pi\pi^*$ and Rydberg in both cases) are included in the wave function. Still, the MS treatment at the MS-RASPT2 level is required to get correct energies and MO extensions.

RASPT2 allows for enlarging the active space with additional MOs, for instance, the σ valence space (5σ, $5\sigma^*$), and these were incorporated into RAS1 and RAS3 spaces in the calculations labeled RASPT2(12,3,3;5,2,1)(SDT) in Table 3. New states, such as $\sigma\pi^*$, $\pi\sigma^*$, $\sigma\sigma^*$, or σRydberg* can now be described by this method, but not only that. At the RASPT2(12,3,3;5,2,16)(SDT) level, the valence−Rydberg mixing is already solved, and the multistate treatment is not required. As observed, two additional σ^* MOs were finally added to the RAS3 space in order to avoid large intruder state problems. Apart from that, the inclusion of the remaining valence electron and orbitals in the active space was sufficient to provide an improved wave function and final results within 0.05 eV from experimental results. This type of behavior has been observed before when active spaces were enlarged to include correlation effects between MOs of different angular moments.[34] Notice that neither the Rydberg nor the $\sigma\sigma^*$ MOs are included in RAS2.

Therefore, in order to incorporate simultaneously the effects of these MOs, a SD excitation level was insufficient (leading to deviations larger than 2 eV) because of the lack of balance between the ground and excited states, as shown in the previous section for FBP. We used one strategy which worked for FBP to balance the treatment; namely, we increased the level of excitation to SDT. Another option would have been to put all the MOs in RAS2, but this would have been unaffordable in this case. We can conclude that RASPT2 provides two different solutions to the valence−Rydberg mixing problem, either reaching the MS level of calculation or introducing new MOs into the RAS spaces, if possible.

Table 4 presents a comparison between the CASSCF/CASPT2/MS-CASPT2(2,11) and RASSCF/RASPT2/MS-RASPT2(2,0,1;0,2,9)(S) levels of calculation for the low-lying singlet and triplet valence and Rydberg states in ethene. As in the previous cases, moving the Rydberg orbitals from RAS2 to RAS3, including up to single excitations from RAS1 to RAS3, provides the same type of accuracy as the full inclusion of the Rydberg MOs into RAS2. This recipe is reliable and a much less costly alternative for the simultaneous calculation of valence and Rydberg states, especially useful for larger systems.

3.C. Acenes: Benzene and Naphthalene. In Tables 5, 6, and 7, we report excitation energies for benzene and naphthalene at different levels of theory. In Table 5, valence and Rydberg ($n = 3$ series) singlet excited states of $\pi\pi^*$, $\pi\sigma^*$, and $\sigma\sigma^*$ character calculated with the CASSCF/CASPT2, RASSCF/RASPT2, MS-CASPT2/MS-RASPT2, and CCSD methods are presented. Two RASPT2 strategies have been followed. In the first set of calculations, the six $\pi\pi^*$ valence MOs were left in RAS2, and the nine Rydberg orbitals were placed in RAS3, allowing up to single excitations. As in the case of ethene, no loss of accuracy is observed with respect to CASPT2 when using this procedure, which largely reduces the computational effort. For instance, the active spaces CAS(6,15) and RAS(6,0,1;0,6,9) generate 2345 and 211 CSFs of ^1A_g symmetry, respectively (see also

Table 4. Excitation Energies (eV) of the Singlet and Triplet Valence $\pi\pi^*$ and $n = 3$ Rydberg States of Ethene

	CAS(2,11)[a]			RAS(2,0,1;0,2,9)(S)[b]			
state	CASSCF	CASPT2	MS-CASPT2	RASSCF	RASPT2	MS-RASPT2	exptl[c]
1^1A_g							
1^1B_{3u} (3s)	6.57	7.26	7.26	6.45	7.23	7.23	7.11
1^1B_{1g} (3pσ)	7.17	7.91	7.91	7.05	7.88	7.88	7.80
1^1B_{2g} (3pσ)	7.18	7.91	7.91	7.06	7.89	7.89	7.90
1^1B_{1u} (V)	7.93	8.43	8.04	7.83	8.44	8.13	8.0[d]
2^1A_g (3pπ)	7.83	8.31	8.31	7.72	8.26	8.27	8.28
2^1B_{3u} (3dσ)	8.01	8.81	8.81	7.88	8.78	8.78	8.62
3^1B_{3u} (3dδ)	8.11	8.93	8.93	7.98	8.90	8.90	8.90
1^1B_{2u} (3dδ)	8.11	8.96	8.96	7.98	8.94	8.94	9.05
1^1A_u (3dπ)	8.10	8.93	8.93	7.97	8.91	8.91	
2^1B_{1u} (3dπ)	9.38	8.98	9.38	9.37	9.03	9.35	9.33
1^3B_{1u} (V)	4.30	4.44	4.44	4.18	4.41	4.42	4.36
1^3B_{3u} (3s)	6.49	7.17	7.17	6.36	7.15	7.15	6.98
1^3B_{1g} (3pσ)	7.14	7.87	7.87	7.02	7.86	7.86	7.79
1^3B_{2g} (3pσ)	7.15	7.88	7.88	7.02	7.85	7.85	
2^3A_g (3pπ)	7.31	8.17	8.17	7.19	8.11	8.11	8.15
2^3B_{3u} (3dσ)	7.99	8.79	8.80	7.86	8.77	8.78	8.57
3^3B_{3u} (3dδ)	8.05	8.88	8.89	7.92	8.86	8.86	
1^3B_{2u} (3dδ)	8.08	8.94	8.94	7.95	8.92	8.92	
1^3A_u (3dπ)	8.10	8.94	8.94	7.97	8.92	8.92	
2^3B_{1u} (3dπ)	8.41	9.09	9.10	8.28	9.04	9.04	

[a] CASSCF, CASPT2, and MS-CASPT2 results, two electrons and 11 MOs including the two $\pi\pi^*$ MOs and nine ($n = 3$) Rydberg MOs. [b] RASSCF, RASPT2, and MS-RASPT2 results, two electrons and 11 orbitals including the two $\pi\pi^*$ MOs (in RAS2) and nine ($n = 3$) Rydberg MOs (in RAS3). Only one particle is allowed (S excitations) in RAS3. [c] See ref 7. [d] Estimated vertical excitation energy from earlier theoretical work. See therein, ref 63.

Table 5. Excitation Energies (eV) for the Low-Lying Valence and Rydberg Singlet States of Benzene[a]

			S		SDT			
state	CASPT2[b]	MS-CASPT2[b]	RASPT2[c] (6,0,1;0,6,9)	MS-RASPT2[c,d] (6,0,1;0,6,9)	RASPT2[e] (12,3,3;3,6,12)	MS-RASPT2[d,e] (12,3,3;3,6,12)	CCSD[f]	exptl[g]
V-$\pi\pi^*$								
1^1B_{2u}	4.94	4.94	4.98	4.98	4.72	4.93	5.19	4.90
1^1B_{1u}	6.22	6.21	6.20	6.20	5.83	6.44	6.59	6.20
1^1E_{1u}	7.12	6.92	7.00	6.82	6.72	6.93	7.17	6.94
2^1E_{2g}	8.05	8.05	8.09	8.10	7.93	7.94	9.18	7.8
R-$\pi\pi^*$								
2^1E_{1u} (3pπ)	7.22	7.29	7.28	7.30	7.16	7.39	7.58	7.41
2^1A_{1g} (3dπ)	7.88	7.87	7.94	7.93	7.85	7.87	7.86	7.81
1^1E_{2g} (3dπ)	7.91	7.88	7.95	7.96	7.88	7.85	7.85	7.81
1^1A_{2g} (3pπ)	7.89	7.91	7.93	7.92	7.82	7.84	7.88	
R-$\pi\sigma^*$								
1^1E_{1g} (3s)	6.54	6.54	6.54	6.54	6.50	6.50	6.55	6.33
1^1A_{2u} (3pσ)	7.12	7.12	7.08	7.08	7.10	7.06	6.99	6.93
1^1E_{2u} (3pσ)	7.22	7.22	7.24	7.24	7.18	7.11	7.06	6.95
1^1A_{1u} (3pσ)	7.15	7.15	7.16	7.16	7.11	7.18	7.14	
1^1B_{2g} (3dσ)	7.75	7.79	7.75	7.75	7.67	7.69	7.66	
1^1B_{1g} (3dσ)	7.76	7.79	7.75	7.75	7.68	7.66	7.66	
2^1E_{1g} (3dδ)	7.73	7.72	7.73	7.71	7.69	7.69	7.64	7.54
3^1E_{1g} (3dδ)	7.77	7.76	7.77	7.79	7.71	7.74	7.70	
R-$\sigma\sigma^*$								
3^1E_{2g} (σ3s)					9.08	9.38	9.39	

[a] For degenerated D_{6h} states, two similar values are obtained in D_{2h} in the CASPT2 and RASPT2 steps, unlike in CASSCF or RASSCF, where external constraints avoid the orbital mixing and symmetry breaking. In all cases, the highest-energy solution has been selected. [b] The CAS space differs for each symmetry (see SI). It includes the six valence $\pi\pi^*$ orbitals and those Rydberg orbitals required to obtain the Rydberg states. All energies referred to ground states with the equivalent CAS. [c] RAS1 empty, RAS2 $\pi\pi^*$ valence MOs, and RAS3 including nine ($n = 3$) Rydberg MOs. A single particle (S) allowed in RAS3. [d] A single-root calculation for the 1^1A_g ground state was used in the MS results. [e] Six additional $\sigma\sigma$ electrons and MOs added to RAS1 and RAS3, up to three holes/particles allowed in RAS1/RAS3. [f] Linear response-CCSD calculations.[65] [g] See revision of data in ref 65.

SI). In benzene, because of its high symmetry, the spurious mixing of valence and Rydberg wave functions is not such a problem as it is in ethene, and therefore there is no significant difference when introducing the MS correction, except for symmetries with close-lying valence and Rydberg states like $^1E_{1u}$, where the changes in energies reach up to 0.18 eV. In the second set of calculations, also reported in Table 5, six additional $\sigma\sigma^*$ electrons and MOs have been included, three in RAS1 and three in RAS3, and up to triple excitations have been allowed. These calculations, RASPT2/MS-RASPT2(12,3,3;3,6,12)(SDT), are much more expensive than the previous ones, RASPT2/MS-RASPT2(6,0,1;0,6,9)(S)

Table 6. Excitation Energies (eV) of the Low-Lying Singlet and Triplet Valence $\pi\pi^*$ States of Benzene Optimized at DFT/B3LYP Level Using TZVP Basis Set[a]

	RASPT2(6,m,m;3,0,3)[b]						
state	SD	SD/SDT[c]	SDT	SDTQ	CASPT2[d]	RASPT2[e]	exptl[f]
1^1A_{1g}							
1^1B_{2u} ($\pi\pi^*$)	5.28	5.01	5.02	5.02	5.02	4.93	4.90
1^1B_{1u} ($\pi\pi^*$)	6.39	6.23	6.24	6.34	6.35	6.44	6.20
2^1E_{1u} ($\pi\pi^*$)	7.19	6.80	6.81	6.78	6.89	6.93	6.94
1^1E_{2g} ($\pi\pi^*$)	8.16	7.60	7.61	7.62	7.61	7.94	7.8
1^3B_{1u} ($\pi\pi^*$)	4.48	4.14	4.15	4.13	4.18		3.94
1^3E_{1u} ($\pi\pi^*$)	4.96	4.79	4.80	4.85	4.85		4.76
1^3B_{2u} ($\pi\pi^*$)	4.96	5.47	5.48	5.60	5.61		5.60
1^3E_{2g} ($\pi\pi^*$)	7.82	7.42	7.43	7.26	7.43		7.24−7.74

[a] Leaving the RAS2 space empty is tested in RASPT2. [b] MS-RASPT2(6,m,m;3,0,3)/TZVP, with m being the indicated level of excitation: SD, SDT, or SDTQ, excluding Rydberg orbitals and states. [c] MS-RASPT2(6,2,2;3,0,3)(SD) for the ground state and MS-RASPT2(6,3,3;3,0,3)(SDT) for the excited state. See text. [d] Present MS-CASPT2(6,6)/TZVP, excluding Rydberg orbitals and states. [e] MS-RASPT2(12,3,3;3,6,12)(SDT)/TZVP, including Rydberg orbitals and states. See Table 4. [f] Experimental data. See refs 65 and 66.

(e.g., 927 588 CFSs for ^1A_g states), and a similar accuracy is obtained. They slightly improve the results in conflictive states like the 2^1E_{2g} valence state, predicted at 7.94 eV at this level, for which the experimental value[65] is 7.8 eV. This highly multiconfigurational state is poorly described by CCSD, which yields 9.18 eV, a value 1.4 eV off with respect to experimental results.[65]

The inclusion of the $\sigma\sigma^*$ MOs and electrons also allows the computation of new states. As an illustration, we have computed the 3^1E_{2g} (σ3s) Rydberg state, a single-reference state, for which RASPT2 and CCSD predict a similar excitation energy.[65] Triple excitations have been included in selected cases in order to compute additional $\sigma\sigma^*$ states. As in the ethene and FBP cases, this is one possible strategy to compensate for the loss of balance caused by not including in RAS2 the $\sigma\sigma^*$ MOs relevant for the simultaneous description of the ground and excited states.

Alternatively, those MOs could be added to RAS2 for both states, and then just up to double excitations would be required.

In Table 6, we compare MS-RASPT2(6,m,m;3,0,3), with $m = 2$ (SD), 3 (SDT), or 4 (SDTQ), to MS-CASPT2(6,6).

Additionally, one set of calculations using SD for the ground and SDT for the excited states has been included. Only the valence $\pi\pi^*$ states are considered. In RASPT2, the RAS2 space was left empty. Inclusion of only up to double excitations leads to errors of about 0.5 eV toward high energies, both in singlet and triplet states. As already shown in FBP, this deviation is due to the lack of balance between the ground and excited states, because the relevant MOs required describing the excited states are excluded from RAS2. To partially correct for this unbalance, we have used the strategies already shown for FBP: either combining SD for the ground state and SDT for the excited states or using SDT or SDTQ for all states. This is a useful comparison between various RASPT2 partitions and the equivalent CASPT2 treatment. In order to reproduce the experimental values, the simultaneous inclusion of Rydberg basis functions, MOs, and states would be required, even to treat valence states only. In conclusion, the strategy of leaving RAS2 empty does not provide extremely accurate results unless a high RAS1/RAS3 excitation level is employed, and it is especially inadequate if only SD is used for all states. Depending on the individual case, it might be preferable either to include in RAS2 the relevant orbitals (see the FBP case) or to increase the excitation level (SDT seems to work for benzene).

Similar comparisons are presented in Table 7 for the singlet and triplet valence $\pi\pi^*$ states of naphthalene. MS-RASPT2 calculations, in which the $\pi\pi^*$ MOs and electrons are placed in RAS1 and RAS3 and RAS2 is left empty, compare reasonably well with the MS-CASPT2(10,10) valence results, but only when at least up to triple (SDT) excitations are considered (at least for the excited states). Otherwise, just by including double excitations (SD), deviations up to 0.8 eV are observed, for instance, for the 2^1B_{3u} state (results not included here). The addition of quadruple excitations (SDTQ) has a large effect on the higher-lying singlet states. As for prior cases, we emphasize two aspects: (i) the lack of the relevant MOs in the RAS2 space provides a poor reference description, and (ii) the valence space alone (in the absence of Rydberg MOs) cannot be used to get accurate values with respect to experimental results, except for the lowest-lying states. In Table 7, we also report previous CASPT2(10,11) results in which Rydberg MOs and states were considered.[67] In this case, the CASPT2/RASPT2 method yields its expected level of accuracy, 0.1−0.3 eV.

At this point, we should notice that it is not possible to make a direct comparison between the old calculations and the present ones because, besides the use of Rydberg orbitals in the old calculations, the IPEA shift is not the same (see Computational Details). However, we still report the old results because it is always useful to collect in a single document several results on the same system, and the old results are more directly comparable to experimental results because of the presence of the Rydberg basis functions in the basis set and Rydberg orbitals in the active space. The same is also true for all results reported in Tables 8−17.

3.D. Heterocyclic Compounds: Furan, Pyrrole, Pyridine, Pyrazine, and Pyrimidine. As for prior cases, the calculations on these organic heterocyclic molecules have the purpose of establishing the accuracy of the partition in which the RAS2 space is left empty, while the valence $\pi\pi^*$ electrons and MOs are located in RAS1 and RAS3. This partition is very appealing because of its simplicity and its great potential for larger systems, but it requires careful checking. Once again the comparison will be performed toward valence CASPT2 calculations, in which the full valence space ($\pi\pi^*$ and n lone-pair MOs) was included in the CAS. The comparison toward the experimental values would require the simultaneous inclusion of Rydberg MOs and states, as shown previously.[63] Technical details about the calculations are reported in the SI.

An inspection of Tables 8 (furan) and 9 (pyrrole) shows that the RASPT2(6,m,m;3,0,2) calculations increase their accuracy with respect to valence CASPT2 in the order SDT, SD/SDT, and SDTQ (excitation level of RAS1 and RAS3).

Table 7. Excitation Energies (eV) of the Singlet and Triplet Valence $\pi\pi^*$ States of Naphthalene (D_{2h}), Leaving the RAS2 Space Empty

	RASPT2(10,m,m;5,0,5)[a]					
state	SD/SDT[b]	SDT	SDTQ	CASPT2[c]	CASPT2[d]	exptl[e]
1^1A_g						
1^1B_{3u} ($\pi\pi^*$)	4.25	4.29	4.23	4.26	4.03	3.97, 4.0
1^1B_{2u} ($\pi\pi^*$)	4.65	4.69	4.61	4.62	4.56	4.45, 4.7
2^1A_g ($\pi\pi^*$)	5.98	6.02	6.00	6.05	5.39	5.50, 5.52
1^1B_{1g} ($\pi\pi^*$)	5.79	5.83	5.87	5.94	5.53	5.27, 5.22
2^1B_{3u} ($\pi\pi^*$)	5.94	5.98	6.20	6.05	5.54	5.63, 5.55, 5.89
2^1B_{2u} ($\pi\pi^*$)	6.17	6.21	6.12	6.13	5.93	6.14, 6.0
2^1B_{1g} ($\pi\pi^*$)	6.74	6.79	6.35	6.34	5.87	6.01, 6.05
3^1A_g ($\pi\pi^*$)	6.77	6.81	6.66	6.72	6.04	
1^3B_{2u} ($\pi\pi^*$)	3.22	3.26	3.21	3.26	3.04[f]	2.98[f,g]
1^3B_{3u} ($\pi\pi^*$)	0.90	0.94	0.90	0.96	0.80	
1^3B_{1g} ($\pi\pi^*$)	1.22	1.26	1.23	1.27	1.14	1.30 − 1.35[g]
2^3B_{2u} ($\pi\pi^*$)	1.32	1.36	1.41	1.38	1.20	
2^3B_{3u} ($\pi\pi^*$)	1.48	1.52	1.45	1.51	1.36	
1^3A_g ($\pi\pi^*$)	2.22	2.26	2.25	2.28	2.18	2.25[g]
2^3B_{1g} ($\pi\pi^*$)	2.68	2.72	2.72	2.70	2.61	3.12[g], 3.0[g]
2^3A_g ($\pi\pi^*$)	3.03	3.07	3.04	3.03	2.73	
3^3A_g ($\pi\pi^*$)	3.15	3.19	3.14	3.17	2.81	2.93[g]
3^3B_{1g} ($\pi\pi^*$)	3.42	3.46	3.40	3.39	3.14	

[a] MS-RASPT2(10,m,m;5,0,5)/TZVP results, with m the indicated level of excitation: SD, SDT, or SDTQ, excluding Rydberg orbitals and states. [b] MS-RASPT2(10,2,2;5,0,5)(SD) for the ground state and MS-RASPT2(10,2,2;5,0,5)(SDT) for the excited state. See text. [c] Present MS-CASPT2(10,10)/TZVP results, excluding Rydberg orbitals and states. [d] CASPT2(10,11), ANO-L 3s2p1d/2s+2s2p2d. Rubio et al.,[67] including Rydberg orbitals and states. [e] Experimental optical data in gas phase and solution: George and Morris,[68] Huebner et al.,[69] Mikami and Ito,[70] Dick and Hohlneicher,[71] Klevens and Platt,[72] Bree and Trirunamachandran.[73] [f] Lowest-lying singlet (1^1A_g)−triplet (1^3B_{2u}) vertical excitation and band absorption maximum. The other excitation energies for the triplet states are referred to the 1^3B_{2u} triplet state. [g] Triplet−triplet absorption experimental data: Hunziker[74,75] and Meyer et al.[76]

Table 8. Excitation Energies (eV) of the Low-Lying Singlet and Triplet Valence $\pi\pi^*$ States of Furan (C_{2v}), Leaving the RAS2 Space Empty

	RASPT2(6,m,m;3,0,2)[a]					
state	SD/SDT[b]	SDT	SDTQ	CASPT2[c]	CASPT2[d]	exptl[e]
1^1A_1						
1^1B_2 ($\pi\pi^*$)	6.55	6.58	6.37	6.28	6.04	6.06
2^1A_1 ($\pi\pi^*$)	6.61	6.64	6.49	6.47	6.16	
3^1A_1 ($\pi\pi^*$)	8.40	8.43	8.05	8.04	7.74	7.82
1^3B_2 ($\pi\pi^*$)	4.51	4.54	4.54	4.28	3.99	4.02
1^3A_1 ($\pi\pi^*$)	5.76	5.79	5.56	5.53	5.15	5.22

[a] MS-RASPT2(6,m,m;3,0,2)/TZVP, with m the indicated level of excitation: SD, SDT, or SDTQ, excluding Rydberg orbital and states. [b] MS-RASPT2(6,2,2;3,0,2)(SD) for the ground state and MS-RASPT2(6,3,3;3,0,2)(SDT) for the excited state. See text. [c] Present MS-CASPT2(6,5)/TZVP, excluding Rydberg orbital and states. [d] CASPT2(6,10), ANO-L 4s3p1d/2s1p+2s2p2d. Serrano-Andrés et al.[63] including Rydberg orbitals and states. [e] Experimental data. Flicker et al.[78]

Table 9. Excitation Energies (eV) of the Low-Lying Singlet and Triplet Valence $\pi\pi^*$ States of Pyrrole (C_{2v}), Leaving the RAS2 Space Empty

	RASPT2(6,m,m;3,0,2)[a]					
state	SD/SDT[b]	SDT	SDTQ	CASPT2[c]	CASPT2[d]	exptl[e]
1^1A_1						
2^1A_1 ($\pi\pi^*$)	6.40	6.54	6.30	6.28	5.92	
1^1B_2 ($\pi\pi^*$)	6.82	6.96	6.67	6.62	6.00	5.98
3^1A_1 ($\pi\pi^*$)	8.18	8.32	7.94	7.92	7.46	7.54
1^3B_2 ($\pi\pi^*$)	4.64	4.78	4.50	4.48	4.27	4.21
1^3A_1 ($\pi\pi^*$)	5.22	5.35	5.29	5.43	5.16	5.10

[a] MS-RASPT2(6,m,m;3,0,2)/TZVP, with m the indicated level of excitation: SD, SDT, or SDTQ, excluding Rydberg orbital and states. [b] MS-RASPT2(6,2,2;3,0,2)(SD) for the ground state and MS-RASPT2(6,3,3;3,0,2)(SDT) for the excited state. See text. [c] Present MS-CASPT2(6,5)/TZVP, excluding Rydberg orbital and states. [d] CASPT2(6,10), ANO-L 4s3p1d/2s1p+2s2p2d,[63] including Rydberg orbitals and states. [e] Experimental data. Flicker et al.,[78] Bavia et al.,[79] and Van Veen.[80]

The RAS(SDTQ) partition typically yields results very close to the full CAS calculation.[77]

Only when reaching a SDTQ level of excitation, which can be prohibitive for larger molecules, can the calculations be considered really accurate. This shows that in some cases it might not be practical to leave RAS2 empty when computing excited states. In order to compare with experimental results, the Rydberg MOs and states may have to be included in the calculation, as shown by previous CASPT2 calculations,[63] whose accuracy was established to be within 0.1 eV.

Tables 10, 11, and 12 provide data for the same type of calculations for the azabenzenes pyridine, pyrazine, and pyrimidine. Both valence $\pi\pi^*$ and $n\pi^*$ states are considered. The performance of RASPT2(10,m,m;5,0,3) versus CASPT2(10,8) is similar to that in the furan and pyrrole cases, although in pyridine the $n\pi^*$ states are less accurately described at the SDT level than at the SD/SDT level. The effect is less pronounced for the other two molecules. In general, we observe that for states below 7.0 eV the deviation of the SDT and SDTQ RAS calculations falls within a value of 0.2 eV compared to valence CASPT2. On the other hand, for higher lying states, the deviation can reach up to 0.5 and 0.3 eV at the SDT and SDTQ levels, respectively. It can be therefore concluded that the empty-RAS2 approach should be used with caution. Even for low-lying roots, a SD or SDT level of excitation may not suffice to obtain a 0.2 eV accuracy, and combining the SD and SDT levels could be a better alternative (considering that extending to SDTQ is

Table 10. Excitation Energies (eV) of the Singlet and Triplet Valence $\pi\pi^*$ and $n\pi^*$ States of Pyridine (C_{2v})

	RASPT2(8,m,m;4,0,3)[a]					
state	SD/SDT[b]	SDT	SDTQ	CASPT2[c]	CASPT2[d]	exptl[e]
1^1A_1						
1^1B_1 ($n\pi^*$)	5.07	5.40	5.15	5.05	4.91	4.59
1^1A_2 ($n\pi^*$)	5.38	5.71	5.42	5.35	5.17	5.43
1^1B_2 ($\pi\pi^*$)	4.74	5.03	5.26	5.10	4.84	4.99
$2\ ^1A_1$ ($\pi\pi^*$)	6.47	6.68	6.71	6.57	6.42	6.38
3^1A_1 ($\pi\pi^*$)	7.31	7.49	7.48	7.12	7.23	7.22
2^1B_2 ($\pi\pi^*$)	7.16	7.10	7.31	7.17	7.48	
4^1A_1 ($\pi\pi^*$)	8.25	8.51	8.47	8.23	7.96	
3^1B_2 ($\pi\pi^*$)	8.07	8.34	8.42	8.21	7.94	
1^3A_1 ($\pi\pi^*$)	4.34	4.67	4.44	4.32	4.05	4.10
1^3B_1($n\pi^*$)	4.52	4.84	4.69	4.50	4.41	
1^3B_2 ($\pi\pi^*$)	4.80	5.09	4.89	4.82	4.56	4.84
2^3A_1 ($\pi\pi^*$)	5.00	5.34	5.18	5.02	4.73	
1^3A_2 ($n\pi^*$)	5.37	5.71	5.42	5.36	5.10	
2^3B_2 ($\pi\pi^*$)	6.40	6.74	6.64	6.69	6.02	
3^3A_1 ($\pi\pi^*$)	7.71	8.04	7.86	7.68	7.34	
3^3B_2 ($\pi\pi^*$)	7.17	7.53	6.97	6.88	7.28	

[a] MS-RASPT2(8,m,m;4,0,3)/TZVP, with m the indicated level of excitation: SD, SDT, or SDTQ, excluding Rydberg orbitals and states. [b] MS-RASPT2(8,2,2;4,0,3)(SD) for the ground state and MS-RASPT2(8,3,3;4,0,3)(SDT) for the excited state. See text. [c] Present MS-CASPT2(8,7)/TZVP, excluding Rydberg orbitals and states. [d] CASPT2(8,12), ANO-L 4s3p1d/2s1p. Lorentzon et al.[81] including Rydberg orbitals and states. [e] Experimental data, Bolovinos et al.[82]

Table 11. Excitation Energies (eV) of the Singlet Valence $\pi\pi^*$ and $n\pi^*$ States of Pyrazine (D_{2h})

	RASPT2 (10,m,m;5,0,3)[a]					
state	SD/SDT[b]	SDT	SDTQ	CASPT2[c]	CASPT2[d]	exptl[e]
1^1A_g						
1^1B_{1u} ($n\pi^*$)	4.06	4.21	3.95	4.09	3.85	3.83
1^1A_u ($n\pi^*$)	4.67	4.82	4.65	4.67	4.63	
1^1B_{2u} ($\pi\pi^*$)	5.02	5.18	4.98	5.04	4.76	4.81
1^1B_{2g} ($n\pi^*$)	5.55	5.71	5.39	5.55		5.46
1^1B_{3g} ($n\pi^*$)	6.50	6.65	6.31	6.47		6.10
1^1B_{3u} ($\pi\pi^*$)	6.61	6.77	6.43	6.68	6.69	6.51
2^1B_{3u} ($\pi\pi^*$)	7.82	7.97	7.46	7.57	7.53	7.67
1^1B_{2u} ($\pi\pi^*$)	7.55	7.70	7.51	7.44	7.74	7.67
1^1B_{1g} ($\pi\pi^*$)	8.33	8.48	8.37	8.43	8.31	
2^1A_g ($\pi\pi^*$)	8.71	8.87	8.67	8.68	8.22	

[a] MS-RASPT2(10,m,m;5,0,3)/TZVP, with m the indicated level of excitation: SD, SDT, or SDTQ, excluding Rydberg orbital and states. [b] MS-RASPT2(10,2,2;5,0,3)(SD) for the ground state and MS-RASPT2(10,3,3;5,0,3)(SDT) for the excited state. See text. [c] Present MS-CASPT2(10,8)/TZVP, excluding Rydberg orbitals and states. [d] CASPT2(10,12), ANO-L 4s3p2d/3s2p. Fülscher and Roos[83] including Rydberg orbitals and states. [e] Experimental data. Innes et al.,[84] Bolovinos et al.,[85] and Okuzawa et al.[86]

actually quite expensive). Otherwise, for higher-lying states, the inclusion of Rydberg orbitals is indispensable.

3.E. DNA/RNA Nucleobases: Adenine, Thymine, Uracil, and Cytosine. In this section, we describe the results of the CASPT2 and RASPT2 study of the DNA/RNA nucleobases adenine, thymine, uracil, and cytosine. We have employed partitions of the RAS spaces similar to those described in the previous section; namely, the valence $\pi\pi^*$ and lone-pair orbitals have been distributed in RAS1 (Hartree−Fock occupied MOs) and RAS3 (Hartree−Fock unoccupied MOs), and RAS2 has been left empty. The results

Table 12. Excitation Energies (eV) of the Singlet Valence $\pi\pi^*$ and $n\pi^*$ States of Pyrimidine (C_{2v})

	RASPT2 (10,m,m;5,0,3)[a]					
state	SD/SDT[b]	SDT	SDTQ	CASPT2[c]	CASPT2[d]	exptl[e]
1^1A_1						
1^1B_1 ($n\pi^*$)	4.13	4.49	4.14	4.33	3.81	3.8 − 4.1
1^1A_2 ($n\pi^*$)	4.58	4.94	4.55	4.71	4.12	4.62
1^1B_2 ($\pi\pi^*$)	5.23	5.35	5.45	5.33	4.23	5.12
2^1A_1 ($\pi\pi^*$)	6.67	7.04	6.96	6.96	6.7	6.7
3^1A_1 ($\pi\pi^*$)	7.71	8.08	7.75	7.54	7.57	7.57
2^1B_2 ($\pi\pi^*$)	7.50	7.60	7.57	7.37	7.32	7.57
4^1A_1 ($\pi\pi^*$)	7.86	8.22	7.82	7.86	7.82	
3^1B_2 ($\pi\pi^*$)	8.61	9.00	8.80	8.76	8.31	8.8

[a] MS-RASPT2(10,m,m;5,0,3)/TZVP, with m the indicated level of excitation: SD, SDT, or SDTQ, excluding Rydberg orbital and states. [b] MS-RASPT2(10,2,2;5,0,3)(SD) for the ground state and MS-RASPT2(10,3,3;5,0,3)(SDT) for the excited state. See text. [c] Present MS-CASPT2(10,8)/TZVP, excluding Rydberg orbitals and states. [d] CASPT2(8,12), ANO-L 4s3p2d/3s2p. Fülscher et al.[87] including Rydberg orbitals and states. [e] Experimental data, Bolovinos et al.[82] See also ref 88.

Table 13. Excitation Energies (eV) of the Singlet Valence $\pi\pi^*$ and $n\pi^*$ States of Adenine (C_s)

	RASPT2 (12,m,m;6,0,4)[a]					
state	SD/SDT[b]	SDT	SDTQ	CASPT2[c]	CASPT2[d]	exptl[e]
$1^1A'$						
$2^1A'$ ($\pi\pi^*$)	5.10	5.18	5.14	5.10	5.13	4.6
$3^1A'$ ($\pi\pi^*$)	5.13	5.21	5.17	5.17	5.20	4.8 − 4.9
$1^1A''$ ($n\pi^*$)	5.07	5.15	4.97	5.15	*f*	5.4
$4^1A'$ ($\pi\pi^*$)	6.34	6.43	6.42	6.41	6.24	5.9 − 6.0
$2^1A''$ ($n\pi^*$)	5.76	5.84	5.78	5.85	6.15	
$5^1A'$ ($\pi\pi^*$)	6.40	6.48	6.47	6.48	6.72	6.3 − 6.4
$6^1A'$ ($\pi\pi^*$)	6.57	6.65	6.63	6.65	6.99	6.8

[a] MS-RASPT2(12,m,m;6,0,4)/TZVP, m indicates level of excitation: SD, SDT, or SDTQ, excluding Rydberg orbitals and states. RAS2 is empty here. [b] MS-RASPT2(12,2,2;6,0,4)(SD) for the ground state and MS-RASPT2(12,3,3;6,0,4)(SDT) for the excited state. See text. [c] Present MS-CASPT2(12,10)/TZVP, excluding Rydberg orbitals and states. [d] CASPT2(12,11), ANO-L 4s3p1d/2s1p,[10] including Rydberg orbitals and states. [e] Experimental absorption data in solution. Mixture with the 7H-adenine tautomer has been noticed. See ref 10 for a critical revision of the experimental results. [f] The active spaces lacked the lowest-lying lone-pair orbital, missing therefore the lowest-lying π^* state.

are compared with full $\pi\pi^*$ and lone-pair valence and valence plus Rydberg CASPT2 calculations and with experimental data.

Table 13 describes the results for the singlet states of adenine. There is an overall agreement within 0.2−0.3 eV among the various sets of calculations. We have not reported here calculations of the type RASPT2(12,2,2;6,0,4)(SD) (RAS2 space empty), which display deviations close to 0.6 eV for some states. It was shown previously that the SD level of excitation is unreliable for excited states if the RAS2 space is not balanced, including, for the states under consideration, the MOs largely modifying their occupation number in the excitation process. The reader must be warned about the comparison of some of the previous CASPT2 results for $n\pi^*$ transitions. In some cases, the proper lone-

Table 14. Excitation Energies (eV) of the Singlet Valence $\pi\pi^*$ and $n\pi^*$ States of Thymine (C_s)

	RASPT2(12,m,m;6,0,3)[a]					
state	SD/SDT[b]	SDT	SDTQ	CASPT2[c]	CASPT2[d]	exptl[e]
$1^1A'$						
$1^1A''$ ($n\pi^*$)	5.01	5.29	5.09	5.24	4.77[f]	
$2^1A'$ ($\pi\pi^*$)	5.64	5.93	5.80	5.56	4.88	4.8 − 5.1
$3^1A'$ ($\pi\pi^*$)	6.61	6.90	6.72	6.54	5.88	6.0 − 6.1
$2^1A''$ ($n\pi^*$)	6.37	6.65	6.43	6.54		
$4^1A'$ ($\pi\pi^*$)	6.70	6.98	6.73	6.58	6.10	6.5 − 6.6
$5^1A'$ ($\pi\pi^*$)	7.59	7.87	7.38	7.19	7.13	6.9 − 7.0

[a] MS-RASPT2(12,m,m;6,0,3)/TZVP, m indicates the level of excitation: SD, SDT, or SDTQ, excluding Rydberg orbitals and states. RAS2 is empty here. [b] MS-RASPT2(12,2,2;6,0,3)(SD) for the ground state and MS-RASPT2(12,3,3;6,0,3)(SDT) for the excited state. See text. [c] Present MS-CASPT2(12,9)/TZVP, excluding Rydberg orbitals and states. [d] CASPT2(12,11), ANO-L 4s3p1d/2s. Lorentzon et al.,[89] including Rydberg orbitals and tates. [e] Experimental absorption data in gas phase and solution. See ref 89 for a critical revision of the experimental results. [f] See ref 90.

Table 15. Excitation Energies (eV) of the Singlet Valence $\pi\pi^*$ and $n\pi^*$ States of Uracil (C_s)

	RASPT2(12,m,m;6,0,3)[a]					
state	SD/SDT[b]	SDT	SDTQ	CASPT2[c]	CASPT2[d]	exptl[e]
$1^1A'$						
$1^1A''$ ($n\pi^*$)	5.19	5.36	5.56	5.43	4.80	
$2^1A'$ ($\pi\pi^*$)	5.84	6.01	5.93	5.90	5.00	4.8 − 5.1
$3^1A'$ ($\pi\pi^*$)	6.64	6.82	6.65	6.73	5.82	6.0 − 6.1
$2^1A''$ ($n\pi^*$)	6.63	6.80	6.90	6.78	6.20	
$4^1A'$ ($\pi\pi^*$)	6.79	6.96	6.87	6.93	6.46	6.5 − 6.6
$5^1A'$ ($\pi\pi^*$)	7.58	7.75	7.38	7.48	7.00	6.9 − 7.0

[a] MS-RASPT2(12,m,m;6,0,3)/TZVP, m indicates the level of excitation: SD, SDT, or SDTQ, excluding Rydberg orbitals and states. RAS2 is empty here. [b] MS-RASPT2(12,2,2;6,0,3)(SD) for the ground state and MS-RASPT2(12,3,3;6,0,3)(SDT) for the excited state. See text. [c] Present MS-CASPT2(12,9)/TZVP, excluding Rydberg orbitals and states. [d] CASPT2(12,11), ANO-L 4s3p1d/2s. Lorentzon et al.,[89] including Rydberg orbitals and sates. [e] Experimental absorption data in gas phase and solution. See ref 89 for a critical revision of the experimental results.

Table 16. Excitation Energies (eV) of the Singlet Valence $\pi\pi^*$ and $n\pi^*$ States of Cytosine (C_s)

	RASPT2 (12,m,m;6,0,3)[a]					
state	SD/SDT[b]	SDT	SDTQ	CASPT2[c]	CASPT2[d]	exptl[e]
$1^1A'$						
$2^1A'$ ($\pi\pi^*$)	4.53	4.96	5.04	4.72	4.39	4.4 − 4.6
$1^1A''$ ($n_O\pi^*$)	5.49	5.92	5.85	5.52	5.00	
$2^1A''$ ($n_N\pi^*$)	5.72	6.15	6.03	5.73	5.06[f]	
$3^1A'$ ($\pi\pi^*$)	5.79	6.22	6.29	5.95	5.36	5.0 − 5.5
$4^1A'$ ($\pi\pi^*$)	6.75	7.17	7.30	6.85	6.16	5.8 − 6.3
$5^1A'$ ($\pi\pi^*$)	7.01	7.43	7.37	7.00	6.74	6.7 − 7.1

[a] MS-RASPT2(10,m,m;6,0,3)/TZVP; m indicates the level of excitation: SD, SDT, or SDTQ, excluding Rydberg orbitals and states. RAS2 is empty here. [b] MS-RASPT2(12,2,2;6,0,3)(SD) for the ground state and MS-RASPT2(12,3,3;6,0,3)(SDT) for the excited state. See text. [c] Present MS-CASPT2(12/9)/TZVP, excluding Rydberg orbitals and states. [d] CASPT2(10,12), ANO-L 4s3p1d/2s.[91] including Rydberg orbitals and states. [e] Experimental absorption data in gas phase and solution. See ref 91 for a critical revision of the experimental results. [f] See ref 3. The corresponding lone pair is missing in the active space in ref 91.

pair MO was left outside the active space, and the corresponding state was therefore missing. This is not due to an inaccuracy of the CASPT2 method but instead to a bad selection of the active space.

Table 17. Comparison between CASPT2 and RASPT2 Excitation Energies (eV) of the Excited States of the Nickel Atom[a]

	CASPT2	CASPT2	RASPT2(10,0,m;0,6,5) (3s3p)3d4s4d[b]			
States	3d4s[b]	3d4s4d[b]	SD	SDT	SDTQ	exptl[c]
^3D ($3d^94s^1$)	0.00	0.00	0.00	0.00	0.00	0.00
^3F ($3d^84s^2$)	−0.33	−0.10	0.01	−0.03	0.04	0.03
^1D ($3d^94s^1$)	0.01	0.28	0.29	0.24	0.24	0.33
^1D ($3d^84s^2$)	1.16	1.45	1.52	1.52	1.61	1.59
^1S ($3d^{10}$)	−0.97	1.79	2.16	2.21	2.01	1.74
^3P ($3d^84s^2$)	1.48	1.68	1.79	1.76	1.85	1.86
^1G ($3d^84s^2$)	2.33	2.54	2.63	2.62	2.71	2.65

[a] The RAS partition is 3d4s in RAS2 and 4d in RAS3, with RAS1 empty, RAS(10,0,m;0,6,5), and different excitation levels in RAS3. Core−valence correlation is computed at the perturbative level (3s3p electrons). [b] CASPT2 and RASPT2(10,0,m;0,6,5) with 18 electrons correlated, basis set ANO-RCC 7s6p4d3f2g, SA(15) for triplet states and SA(19) for singlet states except $^1S(3d^{10})$, a single root calculation. [c] Experimental data. NIST (national institute of standards and technology).[94]

The results on thymine and uracil in Tables 14 and 15 show different trends. In both cases, the RASPT2(SD) level with RAS2-empty was insufficient to get quantitative results. The SDTQ level of excitation is indispensable, which is unfeasible for larger systems. Alternatively, it is better to balance the calculations using SD for the ground state and SDT for the excited states. For higher-lying states, for instance, in the $2^1A'$ and $3^1A'$ $\pi\pi^*$ states, large discrepancies are found between the valence−Rydberg CASPT2 results and the experimental values. The effect is even more clear for both the $\pi\pi^*$ and $n\pi^*$ states of uracil, which is related to the absence of the Rydberg MOs from the active space. The advice would be to add the Rydberg MOs and avoid the MS procedure if the diffuse MOs are not included, because it might lead to overestimated interactions, as was proved previously.[34]

Table 16 displays the results on cytosine, and the conclusions are similar to those obtained for the previous pyrimidine nucleobases. In this case, the SD(ground state)/SDT(excited state) strategy becomes particularly accurate as compared to that with full CASPT2. This strategy could be a cheap alternative in cases where larger RAS2 spaces or high excitation (SDTQ) levels are unfeasible. Once again, one should emphasize the need to include Rydberg MOs and states for calculations on high-lying excited states. For low-lying states, the Rydberg MOs may be excluded, but then the use of the multistate approach is not recommended, because it might lead to spurious interactions.

3.F. Transition Metal Compounds and the Double d-Shell Effect: The Nickel Atom and the Copper Tetrachloride Dianion. Because of the strong correlation effects associated with the 3d shell in first-row transition metals (TM), the inclusion of a second correlating d shell (4d) in the active space was shown to have crucial effects on the relative state energies obtained from CASPT2 for molecules containing first-row transition metal atoms with

a more than a half-filled 3d shell.[33,36,43,92,93] This effect, referred to as the double d-shell effect, is manifested in particular when dealing with transitions between states with a different 3d occupation number, e.g., 3d→4s transitions or charge-transfer (CT) transitions. The double d-shell effect was first reported in a CASPT2 study of the low-lying states of the nickel atom.[36] Here, we report the results of a comparative CASPT2/RASPT2 study of the lowest states in the electronic spectra of the nickel atom and the copper tetrachloride dianion ($CuCl_4^{2-}$). The underlying motivation of this study is to check whether it might be possible to treat the double d-shell effect by means of the much cheaper RASPT2 strategy by, for instance, moving the 4d shell into RAS3. This would allow for applicability of the present multiconfigurational approach to more extended and complex TM systems that have so far been inaccessible or could only be treated qualitatively, because of size limitations of the CASSCF active space, e.g., systems with multiple TM centers.[95]

The calculated results obtained for the spectrum of the Ni atom are presented in Table 17 and compared to experimental results. The first two columns show the CASPT2 relative energies obtained with an active space containing 10 electrons in either the minimum valence active space (3d, 4s) or extended with an extra d shell (3d, 4s, 4d). The double d-shell effect is clearly illustrated by these results. The CASPT2 excitation energies obtained without a second d shell in the active space strongly deviate from the experimental data by 0.3−0.5 eV for all states except ^1S ($3d^{10}$), for which an exceptionally large error of as much as 2.7 eV is found. After including the second d-shell, the errors are reduced to 0.2 eV for all calculated states. These results might be further improved by also including the (4p) shell into the active space, and by further extending the basis set.

The next three columns in Table 17 give the results obtained from RASPT2(10,0,m;0,6,5), with m being the electrons allowed in RAS3, representing a maximum excitation level from two (SD) up to four (SDTQ). Because of the poor convergence of the RASSCF orbital optimization, the RASSCF(SDT) and RASSCF(SDTQ) energies have been calculated at the CI level without orbital optimization, and using the molecular orbitals converged at the RASSCF(SD) level. As one can see, even at the SD level, the double-shell effect is described reasonably well for most states, the results deviating by at most 0.1 eV with respect to the full CASPT2 results. Minor oscillations are observed when increasing the excitation level to SDT and further to SDTQ, but in general there is no clear sign of a systematic improvement. An exception is again the ^1S ($3d^{10}$) state. Here, going from CASPT2 to RASPT2 leads to a significant deterioration of the results, by 0.37 eV at the SD level, and decreasing to 0.22 eV at the SDTQ level. However, it is clear that for this state the RASPT2 description of the double d-shell effect is not converged with respect to the excitation level, and higher levels of excitations are necessary for obtaining quantitative accuracy.

As a final set of calculations, we include here the study at the CASPT2 and RASPT2 levels of the excitation energies of the ligand field (LF) states and a charge transfer (CT) state in the electronic spectrum of the copper tetrachloride dianion ($CuCl_4^{2-}$). In order to compare the results with previous reports,[57,96] the same geometry (planar, D_{4h}, with the Cl ligands on the *x* and *y* axes) and basis sets were used. The valence electronic structure of this molecule is presented in Figure 2. The ground state (GS), 1^2B_{1g}, has a singly occupied molecular orbital (SOMO), σ-antibonding with predominant Cu $3d_{x^2-y^2}$ character, and the lowest part in the spectrum is built from excitations of an electron out of each of the other four 3d orbitals, giving rise to three ligand field (LF) states 1^2B_{2g}, 1^2E_g, and 1^2A_{1g}. An important charge-transfer (CT) state, 2^2B_{1g}, corresponding to an excitation out of the bonding counterpart of the ground state SOMO is also included in the calculations. This CT state belongs to the same symmetry representation as the ground state, and it was shown previously[40] that the interaction between both states resulting from a MS-CASPT2 treatment gives rise to a strongly enhanced covalent character of the GS Cu−Cl σ bonds, by increasing the chlorine $2p\sigma$ contribution in the GS b_{1g}* SOMO. The purpose of the present study is therefore not only to investigate whether the electronic spectrum of $CuCl_4^{2-}$ may be satisfactorily reproduced by means of a RASPT2 rather than a CASPT2 treatment but also to see whether the same covalency enhancing effect for the GS may be obtained from a MS-RASPT2 treatment. The latter may be evaluated by comparing the Mulliken spin populations from the CASSCF and perturbed modified (PM) CASSCF GS wave functions obtained before and after the multistate treatment, respectively.

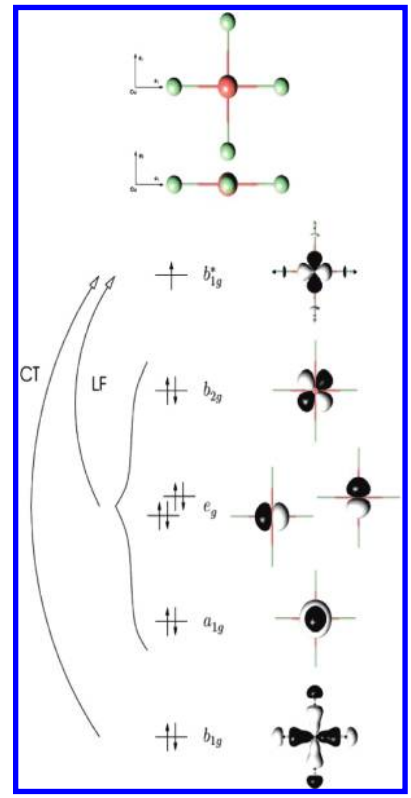

Figure 2. Schematic representation of the geometry and electronic structure of $[CuCl_4]^{2-}$.

The CASPT2 calculations are based on an active space of 11 orbitals, consisting of the Cu 3d and 4d shells together with the bonding b_{1g} orbital. In the RASPT2 calculations,

Table 18. Excitation Energies (eV) of $CuCl_4^{2-}$ Computed at the CASPT2(11,11) and RASPT2(11,0,n;0,6,5) Levels of Calculation Compared with the Available Experimental Data

states	SS-CASPT2 (11,11)	MS-CASPT2 (11,11)	SS-RASPT2(11,0,m;0,6,5) SD	SDT	SDTQ	MS-RASPT2(11,0,m;0,6,5) SD	SDT	SDTQ	exptl[a]
				1^2B_{1g} (GS)					
1^2B_{2g} (LF)	1.52	1.65	1.36	1.48	1.52	1.51	1.63	1.67	1.55
1^2E_g (LF)	1.77	1.90	1.60	1.72	1.76	1.75	1.87	1.91	1.76
1^2A_{1g} (LF)	2.00	2.13	1.91	1.92	1.99	2.06	2.07	2.14	
2^2B_{1g} (CT)	4.60	4.86	4.51	4.52	4.42	4.81	4.81	4.73	

[a] See refs 57, 96.

the correlating 4d shell was transferred into RAS3, leaving RAS1 empty and the other six orbitals in RAS2. This then gives results of the type RASPT2(11,0,m;0,6,5), with m representing the RAS2→RAS3 excitation level. The calculated excitation energies obtained from either a single-state (SS) or multistate (MS) treatment are presented in Table 18. Looking at the SS results first, we note that for the LF states, the results obtained from RASPT2-SDTQ calculations are virtually indistinguishable from CASPT2. A deterioration of the results is observed when decreasing the RASSCF excitation level to SDT and further to SD, although the accuracy of the results obtained from the latter treatment, within 0.2 eV, is still acceptable. On the other hand, for the CT states, the RASPT2 treatment seems to be more problematic, giving an excitation energy that deviates more from the CASPT2 results as the level of excitation is increased. Only two of the states included in the calculations belong to the same B_{1g} representation. A MS treatment will therefore leave the total energy of the other states unaffected, while stabilizing the 1^2B_{1g} ground state and destabilizing the 2^2B_{1g} CT state. This then gives rise to a calculated MS-CASPT2 spectrum in which all three LF states are raised in energy by the same amount, 0.13 eV, as compared to SS-CASPT2, while the 2^2B_{1g} CT state is raised by twice this amount. The results obtained from MS-RASPT2 follow the same trend with respect to SS-RASPT2. As such, the same conclusions concerning the accuracy obtained from RASPT2 for the LF and CT states may be drawn from Table 18, as already noted for the SS results. As compared to the experimental excitation energies for the 1^2B_{2g} and 1^2E_g (LF) states, the SS treatment yields better excitation energies than MS-CASPT2. The addition of the MS step does not increase the accuracy of the results at any of the levels, CASPT2 or RASPT2. This is not unexpected because the active space requirements with MS are larger than for the lower-level methods. It has been shown before that the addition of angular correlation, that is, the inclusion of orbitals with different angular momentum quantum numbers in the active space, largely improves the MS results.[34]

It should finally be mentioned that the RASSCF calculations also reproduce the CASSCF Mulliken spin populations for all states (see SI). In particular, for the ground state, the spin population on copper obtained from RASSCF, 0.84, reflects a very ionic Cu−Cl bond. As was shown in a previous study,[57] this ionic description gives rise to calculated EPR g factors that deviate considerably more from the free-electron value than is observed from experimental results. A significant improvement of the calculated g factors may be obtained by making use instead of the PM CASSCF wave function, giving rise to a more covalent description of the Cu−Cl bonds, with a Mulliken spin population on copper that is decreased by 7%, thus approaching the value of 0.62 ± 0.02 deduced from experimental results.

The most important conclusion to be drawn from the results obtained in this section is that, in general, moving the 4d shell into the RAS3 space is a good strategy that leads to much less expensive calculations in transition metal systems without a considerable loss in accuracy. This then allows for the extension of the methodology to larger systems, both increasing the number of transition metal atoms or including additional ligand molecules. For instance, the number of CSFs decreases from near 98 000 in a CASSCF(10,11) calculation to 4300, 19 000, and 47 500 at the RASSCF(SD), SDT, and SDTQ levels, respectively (for the Ni calculations, see SI).

4. Summary and Conclusions

The electronic excited states of a number of organic (free base porphin, ethene, benzene, naphthalene, furan, pyrrole, and several azobenzenes and nucleobases) and inorganic (the nickel atom and the copper tetrachloride dianion) systems have been computed at the RASSCF/RASPT2/MS-RASPT2 (RAS) levels of calculation using different active space partitions and strategies. The results have been compared to those obtained with well-established procedures like CASSCF/CASPT2/MS-CASPT2 (CAS) or CCSD, and to experimental values, in order to determine the accuracy of several procedures used to divide the RAS space. Our main goal was to establish computational strategies that would provide the most accurate results at reasonable computational costs that one could eventually employ for larger systems. The RAS approaches have many possible ways to define the active spaces for the multiconfigurational calculation, and therefore systematic selection procedures have to be developed and calibrated.

Free base porphin has been first investigated with several partition procedures. RASPT2 has proved to be an excellent strategy to avoid arbitrary divisions of the π space in a system in which the full-π active space (26 electrons in 24 MOs) is out of reach for the CASPT2 method. It has been shown that in the RASPT2 method the proper definition of the RAS2 space (in which a full-CI is performed to define the configurational reference space) is crucial to assessing the accuracy of the calculations. In particular, an initial analysis of the occupation numbers displayed by the relevant MOs, even at a simple RASSCF(SD) level of calculation, is very useful to determine the composition of RAS2. When

computing a RASPT2 energy difference, the highest accuracy is obtained when the MOs changing their occupation number from one state (typically the ground state) to the other (an excited state) the most are simultaneously included in the RAS2 space, leaving the other less significant MOs in the RAS1/RAS3 spaces. If this requirement is fulfilled, a single−double (SD) level of excitations in these two latter active spaces partitions is sufficient to get a high accuracy. In free base porphin, as is typical in many other π organic systems, Gouterman's four MOs (HOMO, HOMO−1, LUMO, and LUMO+1) form the basic set required to describe the four low-lying $\pi\pi^*$ excited states, and therefore it will be sufficient to include them in RAS2 while leaving the remaining $\pi\pi^*$ MOs in RAS1/RAS3 and reaching a SD level of excitation to get accurate results. Higher states will however require extension of the RAS2 space to include additional MOs. It is possible to design a less straightforward strategy and perform calculations for each of the two states with different active spaces. If the proper MOs are excluded from RAS2, the results are unbalanced in the CI treatment, and the second-order perturbation correction may not be able to compensate the results. Particularly for this case, a SD level of excitation is clearly insufficient. Although not as accurate as the inclusion of the proper MOs in RAS2, there are some additional strategies that may help to slightly improve the results even if some important MOs are excluded from RAS2, for instance, using different levels of excitation for the two considered states, like SD for the ground and SDT for the excited state, or increasing the overall excitation as much as possible, SDT, or even better, SDTQ, although these latter strategies might be impossible to apply because of the very large configurational spaces. All of these results open the possibility to use RASPT2 for many organic systems with extended π spaces without a further loss of accuracy due to restrictions in the size of the active space.

Calculations on the valence and Rydberg singlet and triplet excited states of ethene and benzene have illustrated the advantages of RASPT2 versus CASPT2 when large active spaces including both valence and Rydberg states and MOs are required. A new strategy for the active MO partition has been used in which the Rydberg MOs—typically nine (n = 3) for common organic systems—are placed in RAS3, leaving in the RAS2 space the valence $\pi\pi^*$ MOs and electrons, and allowing, apart from the full-CI expansion within RAS2, just single excitations toward RAS3. The advantage of the RAS approach, whose accuracy is similar to that of a full CAS calculation, is that the Rydberg orbitals can be moved out of the RAS2 space. The computational effort is therefore substantially decreased, and the approach can be employed to study systems with large π-valence spaces. Also, the calculations are simpler because they permit the use of a unique space for the different symmetries. This approach, however, does not solve directly the valence−Rydberg mixing problems already found in CASSCF/CASPT2, leading to too high excitation energies and heavily mixed wave functions with too large orbital extensions for some valence states. As previously shown, when only the $\pi\pi^*$ MOs are included in the RAS2 space, the multistate (MS) procedure, MS-RASPT2, is required to solve the mixing and provide orthogonal states with clear valence or Rydberg mixings. In the ethene case, we have also shown that the inclusion of the $\sigma\sigma^*$ MOs in the RAS1 and RAS3 spaces (not possible in general for CAS calculations) opens new possibilities but also brings some problems. Since one cannot include in RAS2 both the $\pi\pi^*$ and $\sigma\sigma^*$ MOs, the RASPT2(SD) level of calculation is not sufficient to correctly describe the $\sigma\sigma^*$ excitations. Increasing the excitation level to SDT solved the problem in the ethene case, although this might not be a general rule. When including both π and σ correlation within the CI reference space, the valence−Rydberg mixing was solved at the RASPT2(SDT) level, without using the MS-RASPT2(SDT) procedure. This shows the importance of electronic correlation in defining the wave function when dealing with the valence−Rydberg mixing problem.

Calculations on different heteroaromatic organic molecules, including furan, pyrrole, and some azabenzenes and nucleobases, have shown that the most computationally advantageous RASPT2 strategy, consisting of leaving the RAS2 space empty and placing the occupied and unoccupied MOs in RAS1 and RAS3, respectively, is, in general, not particularly accurate. For low-lying states, the lack of balance between the ground and excited states caused by the improper definition of RAS2 can be partially compensated if different levels of excitations are used when defining the configurational space, in particular if using SD to compute the ground and SDT to obtain the excited state. The strategy yields poorer results for higher-lying states, mainly because of the effect of the absent Rydberg MOs and states, which should be included in the calculations to obtain accurate results.

Regarding the calculation of the first-row transition metal systems, our main goal was to analyze the effect on the excitation energies of moving the 4d correlating shell from RAS2 to RAS3. The electronic spectra of the nickel atom and the copper tetrachloride dianion have been analyzed. The main conclusion is that, overall, the RASPT2 calculations quite well reproduce the corresponding CASPT2 results (to within 0.1−0.2 eV), although a few exceptional cases were also observed, e.g., the ^{1}S ($3d^{10}$) state of the nickel atom.

Acknowledgment. Research supported by projects CTQ2007-61260, CTQ2010-14892, and CSD2007-0010 Consolider-Ingenio in Molecular Nanoscience of the Spanish MEC/FEDER and the Generalitat Valenciana, by grants from the Flemish Science Foundation (FWO) and the Concerted Research Action of the Flemish Government (GOA) and by the Director, Office of Basic Energy Sciences, U.S. Department of Energy under Contract no. USDOE/DE-SC002183 and University of Minnesota Supercomputing Institute. S.V. thanks the University of Leuven (BOF) for financial support. Discussions with Prof. Per-Åke Malmqvist are deeply acknowledged. After the submission of this paper, one of the coauthors, Luis Serrano-Andrés, passed away unexpectedly. We would like to dedicate this paper to Luis, who will be terribly missed as a friend and as a colleague.

Supporting Information Available: Additional details of the calculations: some of the employed geometries, details of the symmetry restrictions used, sizes of the configurational spaces and Mulliken spin population for the states of the

copper tetrachloride dianion. This information is available free of charge via the Internet at http://pubs.acs.org/.

References

(1) Andersson, K.; Malmqvist, P.-Å.; Roos, B. O. *J. Chem. Phys.* **1992**, *96*, 1218.

(2) Andersson, K.; Roos, B. O. *Int. J. Quantum Chem.* **1993**, *45*, 591.

(3) Merchán, M.; Serrano-Andrés, L. *J. Am. Chem. Soc.* **2003**, *125*, 8108.

(4) Hrovat, D. A.; Morokuma, K.; Borden, W. T. *J. Am. Chem. Soc.* **1994**, *116*, 1072.

(5) Lindh, R.; Persson, B. J. *J. Am. Chem. Soc.* **1994**, *116*, 4963.

(6) Moriarty, N. W.; Lindh, R.; Karlstrom, G. *Chem. Phys. Lett.* **1998**, *289*, 442.

(7) Serrano-Andrés, L.; Merchán, M.; Nebotgil, I.; Lindh, R.; Roos, B. O. *J. Chem. Phys.* **1993**, *98*, 3151.

(8) Serrano-Andrés, L.; Lindh, R.; Roos, B. O.; Merchán, M. *J. Phys. Chem.* **1993**, *97*, 9360.

(9) Serrano-Andrés, L.; Roos, B. O. *J. Am. Chem. Soc.* **1996**, *118*, 185.

(10) Fülscher, M. P.; Serrano-Andrés, L.; Roos, B. O. *J. Am. Chem. Soc.* **1997**, *119*, 6168.

(11) La Macchia, G.; Li Manni, G.; Todorova, T. K.; Brynda, M.; Aquilante, F.; Roos, B. O.; Gagliardi, L. *Inorg. Chem.* **2010**, *49*, 5216.

(12) Radoń, M.; Pierloot, K. *J. Phys. Chem. A* **2008**, *112*, 11824.

(13) Creve, S.; Pierloot, K.; Nguyen, M. T.; Vanquickenborne, L. G. *Eur. J. Inorg. Chem.* **1999**, 107.

(14) Persson, B. J.; Roos, B. O.; Pierloot, K. *J. Chem. Phys.* **1994**, *101*, 6810.

(15) Pierloot, K.; Persson, B. J.; Roos, B. O. *J. Phys. Chem.* **1995**, *99*, 3465.

(16) Roos, B. O.; Borin, A. C.; Gagliardi, L. *Angew. Chem., Int. Ed.* **2007**, *46*, 1469.

(17) Gagliardi, L.; Roos, B. O. *Inorg. Chem.* **2003**, *42*, 1599.

(18) Pierloot, K.; Van Praet, E.; Vanquickenborne, L. G.; Roos, B. O. *J. Phys. Chem.* **1993**, *97*, 12220.

(19) Pierloot, K.; Tsokos, E.; Vanquickenborne, L. G. *J. Phys. Chem.* **1996**, *100*, 16545.

(20) Pierloot, K.; De Kerpel, J. O. A.; Ryde, U.; Roos, B. O. *J. Am. Chem. Soc.* **1997**, *119*, 218.

(21) Pierloot, K.; De Kerpel, J. O. A.; Ryde, U.; Olsson, M.; Roos, B. O. *J. Am. Chem. Soc.* **1998**, *120*, 13156.

(22) Delabie, A.; Pierloot, K.; Groothaert, M. H.; Schoonheydt, R. A.; Vanquickenborne, L. G. *Eur. J. Inorg. Chem.* **2002**, *3*, 515.

(23) Gagliardi, L.; Roos, B. O. *Chem. Soc. Rev.* **2007**, *36*, 893.

(24) Roos, B. O.; Malmqvist, P. Å.; Gagliardi, L. *J. Am. Chem. Soc.* **2006**, *128*, 17000.

(25) Gagliardi, L. *Theor. Chem. Acc.* **2006**, *116*, 307.

(26) Pierloot, K.; van Besien, E. *J. Chem. Phys.* **2005**, *123*, 204309.

(27) Roos, B. O.; Andersson, K.; Fülscher, M. P.; Malmqvist, P. A.; Serrano-Andrés, L.; Pierloot, K.; Merchán, M. In *Advances in Chemical Physics, Vol XCIII*; John Wiley & Sons Inc: New York, 1996; Vol. 93, p 219.

(28) Serrano-Andrés, L.; Merchán, M.; Rubio, M.; Roos, B. O. *Chem. Phys. Lett.* **1998**, *295*, 195.

(29) Schreiber, M.; Silva, M. R.; Sauer, S. P. A.; Thiel, W. *J. Chem. Phys.* **2008**, *128*, 134110.

(30) Ghigo, G.; Roos, B. O.; Malmqvist, P. A. *Chem. Phys. Lett.* **2004**, *396*, 142.

(31) Serrano-Andrés, L.; Merchán, M. *THEOCHEM* **2005**, *729*, 99.

(32) Forsberg, N.; Malmqvist, P. A. *Chem. Phys. Lett.* **1997**, *274*, 196.

(33) Roos, B. O.; Andersson, K.; Fülscher, M. P.; Serrano-Andrés, L.; Pierloot, K.; Merchán, M.; Molina, V. *THEOCHEM* **1996**, *388*, 257.

(34) Serrano-Andrés, L.; Merchán, M.; Lindh, R. *J. Chem. Phys.* **2005**, *122*, 104107.

(35) Finley, J.; Malmqvist, P. A.; Roos, B. O.; Serrano-Andres, L. *Chem. Phys. Lett.* **1998**, *288*, 299.

(36) Andersson, K.; Roos, B. O. *Chem. Phys. Lett.* **1992**, *191*, 507.

(37) Aquilante, F.; Pedersen, T. B.; Lindh, R.; Roos, B. O.; De Meras, A. S.; Koch, H. *J. Chem. Phys.* **2008**, *129*, 8.

(38) Aquilante, F.; Malmqvist, P. A.; Pedersen, T. B.; Ghosh, A.; Roos, B. O. *J. Chem. Theory Comput.* **2008**, *4*, 694.

(39) Aquilante, F.; De Vico, L.; Ferré, N.; Ghigo, G.; Malmqvist, P.-Å.; Pedersen, T.; Pitonak, M.; Reiher, M.; Roos, B. O.; Serrano-Andrés, L.; Urban, M.; Veryazov, V.; Lindh, R. *J. Comput. Chem.* **2010**, *31*, 224.

(40) Aquilante, F.; Gagliardi, L.; Pedersen, T. B.; Lindh, R. *J. Chem. Phys.* **2009**, *130*, 154107.

(41) Pierloot, K.; Vancoillie, S. *J. Chem. Phys.* **2008**, *128*, 034104.

(42) Aquilante, F.; Todorova, T. K.; Gagliardi, L.; Pedersen, T. B.; Roos, B. *J. Chem. Phys.* **2009**, *131*, 7.

(43) Malmqvist, P. Å.; Pierloot, K.; Shahi, A. R. M.; Cramer, C. J.; Gagliardi, L. *J. Chem. Phys.* **2008**, *128*, 204109.

(44) Roos, B. O. In *Ab Initio Methods in Quantum Chemistry*, Part II; Lawley, K. P., Ed.; Wiley: Chicester, U. K., 1987.

(45) Olsen, J.; Roos, B. O.; Jorgensen, P.; Jensen, H. J. A. *J. Chem. Phys.* **1988**, *89*, 2185.

(46) Malmqvist, P.-Å.; Rendell, A.; Roos, B. O. *J. Phys. Chem.* **1990**, *94*, 5477.

(47) Huber, S. M.; Moughal Shahi, A. R.; Aquilante, F.; Cramer, C. J.; Gagliardi, L. *J. Chem. Theory Comput.* **2009**, *5*, 2967.

(48) Moughal Shahi, A. R.; Cramer, C. J.; Gagliardi, L. *Phys. Chem. Chem. Phys.* **2009**, *11*, 10964.

(49) Widmark, P. O.; Malmqvist, P. A.; Roos, B. O. *Theor. Chim. Acta* **1990**, *77*, 291.

(50) Schäfer, A.; Huber, C.; Ahlrichs, R. *J. Chem. Phys.* **1994**, *100*, 5829.

(51) Aquilante, F.; Malmqvist, P.-A.; Pedersen, T. B.; Ghosh, A.; Roos, B. O. *J. Chem. Theory Comput.* **2008**, *4*, 694.

(52) Aquilante, F.; Pedersen, T. B.; Lindh, R. *J. Chem. Phys.* **2007**, *126*, 11.

(53) Aquilante, F.; Pedersen, T. B.; Sanchez de Meras, A.; Koch, H. *J. Chem. Phys.* **2006**, *125*, 174101.

(54) Roos, B. O.; Lindh, R.; Malmqvist, P. A.; Veryazov, V.; Widmark, P. O. *J. Phys. Chem. A* **2005**, *109*, 6575.

(55) Hess, B. A. *Phys. Rev. A* **1986**, *33*, 3742.

(56) Douglas, N.; Kroll, N. M. *Annu. Phys.* **1974**, *82*, 89.

(57) Vancoille, S.; Pierloot, K. *J. Phys. Chem. A* **2008**, *112*, 4011.

(58) Becke, A. D. *J. Chem. Phys.* **1993**, *98*, 5648.

(59) Ahlrichs, R.; Bar, M.; Haser, M.; Horn, H.; Kolmel, C. *Chem. Phys. Lett.* **1989**, *162*, 165.

(60) Merchán, M.; Ortí, E.; Roos, B. O. *Chem. Phys. Lett.* **1994**, *226*, 27.

(61) Gwaltney, S. R.; Bartlett, R. J. *J. Chem. Phys.* **1998**, *108*, 6790.

(62) Serrano-Pérez, J. J.; Serrano-Andrés, L.; Merchán, M. *J. Chem. Phys.* **2006**, *124*, 124502.

(63) Serrano-Andrés, L.; Merchán, M.; Nebotgil, I.; Roos, B. O.; Fulscher, M. *J. Am. Chem. Soc.* **1993**, *115*, 6184.

(64) Serrano-Andrés, L.; Sánchez-Marín, J.; Nebot-Gil, I. *J. Chem. Phys.* **1992**, *97*, 7499.

(65) Christiansen, O.; Koch, H.; Halkier, A.; Jorgensen, P.; Helgaker, T.; Sánchez de Merás, A. *J. Chem. Phys.* **1996**, *105*, 6921.

(66) Halda, K.; Hättig, C.; Jorgensen, P. *J. Chem. Phys.* **2000**, *113*, 7765.

(67) Rubio, M.; Merchán, M.; Ortí, E.; Roos, B. O. *Chem. Phys.* **1994**, *179*, 395.

(68) George, G. A.; Morris, G. C. *J. Mol. Spetrosc.* **1968**, *26*, 67.

(69) Huebner, R. H.; Mielczarek, S. R.; Kuyait, C. E. *Chem. Phys. Lett.* **1972**, *16*, 464.

(70) Mikami, N.; Ito, M. *Chem. Phys. Lett.* **1975**, *31*, 472.

(71) Dick, B.; Hohlneicher, G. *Chem. Phys. Lett.* **1981**, *84*, 471.

(72) Klevens, H. B.; Platt, J. R. *J. Chem. Phys.* **1949**, *17*, 470.

(73) Bree, A.; Trirunamachandran, T. *Mol. Phys.* **1962**, *5*, 397.

(74) Hunziker, H. E. *J. Chem. Phys.* **1972**, *56*, 400.

(75) Hunziker, H. E. *Chem. Phys. Lett.* **1969**, *3*, 504.

(76) Meyer, Y. H.; Astier, R.; Leclerq, J. M. *J. Chem. Phys.* **1972**, *56*, 801.

(77) Serrano-Andrés; L.; Roos, B. O. *Chem. Eur. J.* **1997**, *3*, 717.

(78) Flicker, W. M.; Mosher, O. A.; Kuppermann, A. *J. Chem. Phys.* **1976**, *64*, 1315.

(79) Bavia, M.; Bertinelli, F.; Taliani, C.; Zauli, C. *Mol. Phys.* **1976**, *31*, 479.

(80) Van Veen, E. H. *Chem. Phys. Lett.* **1976**, *41*, 535.

(81) Lorentzon, J.; Fülscher, M. P.; Roos, B. O. *Theor. Chim. Acta* **1995**, *92*, 67.

(82) Bolovinos, A.; Tsekeris, P.; Philis, J.; Pantos, E.; Andritsopoulus, G. *J. Mol. Spetrosc.* **1984**, *103*, 240.

(83) Fülscher, M. P.; Roos, B. O. *Theor. Chim. Acta* **1994**, *87*, 403.

(84) Innes, K. K.; Ross, I. G.; Moomaw, W. R. *J. Mol. Spetrosc.* **1988**, *132*, 49.

(85) Bolovinos, A.; Tsekeris, P.; Philis, J.; Pantos, E.; Andritsopoulus, G. *Chem. Phys.* **1990**, *147*, 19.

(86) Okuzawa, Y.; Fujii, M.; Ito, M. *Chem. Phys. Lett.* **1990**, *171*, 341.

(87) Fülscher, M. P.; Andersson, K.; Roos, B. O. *J. Phys. Chem.* **1992**, *96*, 9204.

(88) Malmqvist, P.-Å.; Roos, B. O.; Fülscher, M. P.; Rendell, A. *Chem. Phys.* **1992**, *162*, 359.

(89) Lorentzon, J.; Fülscher, M. P.; Roos, B. O. *J. Am. Chem. Soc.* **1995**, *117*, 9265.

(90) Serrano-Pérez, J. J.; González-Luque, R.; Merchán, M.; Serrano-Andrés, L. *J. Phys. Chem. B* **2007**, *111*, 11880.

(91) Fülscher, M. P.; Roos, B. O. *J. Am. Chem. Soc.* **1995**, *117*, 2089.

(92) Pierloot, K. In *Computational Organometallic Chemistry*; Cundari, T., Ed.; Marcel Dekker, Inc.: New York, 2001; p 123.

(93) Pierloot, K. *Mol. Phys.* **2003**, *101*, 2083.

(94) Linstrom, P. J.; Mallard, W. G. *NIST Chemistry WebBook, NIST Standard Reference Database Number 69*; National Institute of Standards and Technology: Gaithersburg, MD, 2010.

(95) Vancoillie, S.; Chalupský, J.; Ryde, U.; Solomon, E. I.; Pierloot, K.; Neese, F.; Rulíšek, L. *J. Phys. Chem. B* **2010**, *114*, 7692.

(96) Vancoillie, S.; Malmqvist, P.-Å.; Pierloot, K. *Chem. Phys. Chem.* **2007**, *8*, 1803.

CT100478D